Development of a multi-component gastroretentive expandable drug delivery system (GREDDS) for personalized administration of metformin

Journal:	*Expert Opinion on Drug Delivery*
Manuscript ID	EODD-2023--0223.R3
Manuscript Type:	Original Research (Invited)
Keywords:	3D printing, fused deposition modeling, prolonged release, viscoelastic behavior, oral administration, diabetes

Development of a multi-component gastroretentive expandable drug delivery system (GREDDS) for personalized administration of metformin

Marco Uboldi[1] (M.U.), Arianna Chiappa[2] (A.C.), Margherita Rossi[2] (M.R.), Francesco Briatico-Vangosa[2,*] (F.B.V.), Alice Melocchi[1,*] (A.M.), Lucia Zema[1] (L.Z.)

[1]Sezione di Tecnologia e Legislazione Farmaceutiche "Maria Edvige Sangalli", Dipartimento di Scienze Farmaceutiche, Università degli Studi di Milano, via G. Colombo 71, 20133 Milano, Italy;

[2]Dipartimento di Chimica, Materiali e Ingegneria Chimica "G. Natta", Politecnico di Milano, Piazza Leonardo da Vinci 32, 20133 Milano, Italy.

* Corresponding authors:

Alice Melocchi - alice.melocchi@unimi.it; 0039 02 503 24665

Francesco Briatico-Vangosa - francesco.briatico@polimi.it; 0039 02 2399 3290

Author contributions

M.U.: Conceptualization, Software, Investigation, Writing - Original Draft

A.C.: Investigation, Data Curation, Writing - Original Draft, Validation

M.R.: Investigation, Data Curation

F.B.V.: Methodology, Formal analysis, Resources, Writing - Review & Editing

A.M.: Conceptualization, Writing - Original Draft, Writing - Review & Editing, Supervision

L.Z.: Resources, Writing - Review & Editing, Supervision, Project administration

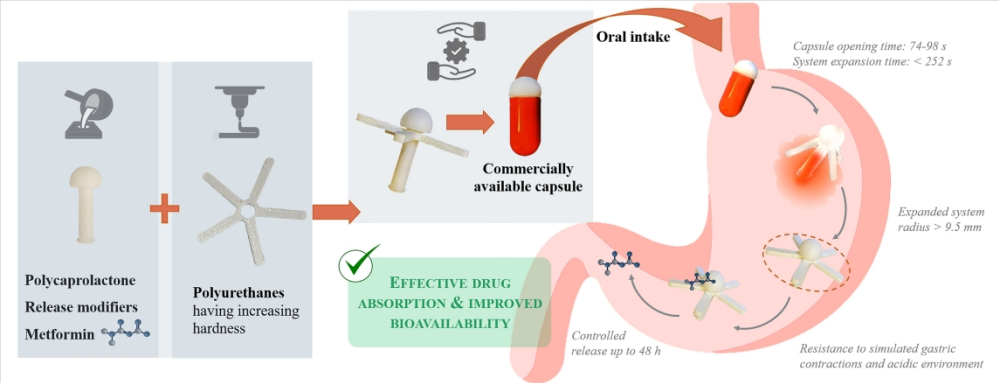

Graphical Abstract

129x49mm (600 x 600 DPI)

Development of a multi-component gastroretentive expandable drug delivery system (GREDDS) for personalized administration of metformin

Article highlights box

- A gastroretentive drug delivery system (DDS) enabling prolonged release of metformin in the upper gastrointestinal tract was designed for type II diabetes therapy, to increase drug bioavailability while improving efficacy and compliance;
- The new DDS was characterized by simplicity of operation/administration/disposal, efficiency of retention/release, and versatility of content/release kinetics;
- The DDS consisted of: a core ensuring prolonged release of metformin, a skeleton responsible for retention into the stomach and a commercial capsule containing these parts properly assembled and enabling administration;
- The form-fit-function approach was applied for designing the components of the DDS and selecting suitable formulations/materials;
- DDS prototypes were assembled using melt-casted polycaprolactone-based cores and 3D printed thermoplastic polyurethanes skeletons.

Abstract

Objectives Efficacy and compliance of type II diabetes treatment would greatly benefit from dosage forms providing controlled release of metformin in the upper gastrointestinal tract. In this respect, the feasibility of a new system ensuring stomach-retention and personalized release of this drug at its absorption window for multiple days was investigated.

Methods The system proposed comprised of a drug-containing core and a viscoelastic umbrella-like skeleton, which were manufactured by melt-casting and 3D printing. Prototypes, alone or upon assembly and insertion into commercially-available capsules, were characterized for key parameters: thermo-mechanical properties, accelerated stability, degradation, drug release, deployment performance and resistance to simulated gastric contractions.

Results Each part of the system was successfully manufactured using purposely-selected materials and the performance of final prototypes matched the desired one. This included: *i)* easy folding of the skeleton against the core in the collapsed administered shape, *ii)* rapid recovery of the cumbersome configuration at the target site, even upon storage and *iii)* prolonged release of metformin.

Conclusions Composition, geometry and performance of the system developed in this work were deemed acceptable for stomach retention and prolonged as well as customizable release of metformin at its absorption window, laying promising bases for further development steps.

Keywords: 3D printing, fused deposition modeling, prolonged release, viscoelastic behavior, oral administration, diabetes

1. Introduction

Interest in gastroretentive drug delivery systems (GRDDSs) can be dated back to the late '80s [1-3]. At that time, researchers investigated a variety of formulation strategies for developing orally administered dosage forms able to control drug release and to remain into the stomach for long times (generally ≥ 8h), despite physiological contractions and presence of food. Over years, GRDDSs were shown a promising solution for providing effective concentrations of different active ingredients, either to exert a local action in the gastric environment (*e.g.* for treating inflammatory diseases as well as for *Helicobacter pylory* eradication) or to improve their systemic absorption [4,5]. In the latter case, they were used to increase the bioavailability of *i)* weakly acidic molecules, which are poorly soluble in basic pHs, and of *ii)* drugs that are primarily absorbed into the stomach or in the first portion of the small intestine. Moreover, ability of GRDDSs to prolong drug release over several days following a single oral intake allowed to enhance therapy adherence, especially when dealing with patients treated with multiple drugs at high quantities and/or with short half-life [6,7]. Indeed, their administration resulted in a simplification of the therapeutic regimen, reducing the number of units taken throughout the day.

Although GRDDSs are well-known to provide high patient compliance and improved bioavailability, in the past years their attainment has represented a major challenge for scientists, probably because technological advancements were needed to ease their manufacturing. Indeed, GRDDSs have recently gained renewed attention within the research community, due to the availability of new materials and the advent of easy-to access as well as versatile manufacturing techniques, such as 3D and 4D printing [8-13]. In this respect, systems with increased complexity were designed not only for conveyance of small molecules but also for delivering biologics *via* the oral route, taking advantage of physical modes typical of transdermal applications (*e.g.* piercing, jetting, ultrasound), [14-22]. The star-shaped drug delivery platform named Lyndra LYNX, which is already under clinical evaluation, represents one of the main examples of the so-called next generation of GRDDSs [23]. Indeed, it was designed to reduce dosing frequency from to once a week to once a month, and

to have broad applicability across multiple therapeutic areas [24-28]. Illnesses that result hard-to-treat and are considered socially and economically impactful - such as altered psychiatric conditions, dyslipidemia, opioid use disorder, pregnancy prevention, malaria eradication and HIV - are among the pathologies that this platform would help managing. Moreover, the implementation of GRDDSs like the Lyndra LYNX platform into medical practice could lead to major reduction of overall healthcare expenses. By way of example, they would reduce the strength of the active ingredient administered, by avoiding its undesired loss associated with release outside the absorption window, and enable more efficient use of available resources [5,17].

In the last decades, prolonged retention within the stomach was attained taking advantage of high-density-, floatation-, adhesion/anchoring- and expansion-based formulation approaches, pursued either alone or in combination [1,29-33]. High-density GRDDSs are generally formulated to contain inert materials to increase the weight/volume ratio of the final product. Being responsible for device settling on below the level of the pylorus, such materials are intended to decrease likelihood of elimination during gastric emptying. Conversely, low density floating systems would remain on top of the stomach content, thus prolong their residence time. For mucoadhesive dosage forms, long-lasting retention is enabled by the presence of a component ensuring their adhesion to the epithelial surface of the target organ. Finally, expansion-based systems (GREDDSs) are actively or passively able to modify their size after swallowing. Once within the gastric environment, they gain a spatial encumbrance greater than the average dimensions of the open pylorus. However, for oral intake by swallowing, they need to present a collapsed shape, from both the functional perspective and the patient psychological point of view. Thus, they are often delivered into commercially-available hard capsules. With respect to the expansion that GREDDSs must necessarily undergo once within the target organ, most of them assume the configuration responsible for retention following either swelling or unfolding processes. While in the former case the desired volume increase is triggered by absorption of water/biological fluids, various unfolding approaches have been investigated over years, especially to ensure transition from the collapsed to the expanded shape in the shortest possible

time. Such strategies mainly involved mechanical/elastic deployment, shape memory effect and superelasticity [5,34,35]. By way of example, the unique superelastic behavior of nitinol was used for manufacturing a necklace-like device able to convey high drug dosages covering multiple weeks of treatment [36,37]. In the same way, by using shape memory polymers as feedstock material for 3D printing, the novel concept of 4D printing was preliminarily tested for the production of systems intended for retention within various hollow-muscular organs [38-44].

Type II diabetes is one of the most widespread pathologies in high-income countries, generating major healthcare expenses if not well-managed [45]. Metformin hydrochloride generally represents the first-line drug for newly diagnosed diabetic patients, because of its high efficacy, safety, tolerability and limited cost [46-51]. Indeed, it not only prevents rise in blood glucose by decreasing insulin resistance, but also reduces glycated hemoglobin without incurring hypoglycemic episodes. Moreover, metformin is able to provide other extra-glycemic effects that would be beneficial for people suffering from diabetes. Indeed, it protects against cardiovascular risk, which generally increases over time if hyperglycemia is not well-controlled, and favors loss of body weight. Currently, metformin is mainly formulated in immediate release (IR) dosage forms for oral consumption. However, drug bioavailability resulting from this administration mode is about 56%, because part of the active ingredient is lost, being not properly available where it is mostly absorbed, *i.e.* in the upper gastrointestinal tract [42-57]. Therefore, controlled release of metformin at its absorption window could be highly beneficial. However, its high water solubility (300 mg/mL) as well as short half-life (40 min) could pose major challenges towards this target [11,58-60]. As a consequence, patients are currently forced to assume the drug several times through the day (generally 500 - 1000 mg taken twice a day), which often leads to nausea, diarrhea, loss of appetite and lactic acidosis due to the burst effect resulting from each administration [61-64]. In addition, during chronic therapy, metformin receptors become less responsive, thus requiring an increase in the administered quantity to maintain the beneficial effects. In this respect, metformin-containing dosage forms ensuring its prolonged release in the upper gastrointestinal tract would represent a major step forward in the current treatment

of diabetes [60]. Besides increasing therapy effectiveness and possibly limiting the risk of patient hospitalization for uncontrolled symptoms, the therapeutic approach involving the use of GRDDSs would have a major impact on the costs associated with diabetes, which in Europe were estimated to be around € 2850 for each subject yearly [65-70].

Based on these premises, the aim of the present work was to design and to preliminarily evaluate the feasibility of a GREDDS with improved potential in the treatment of type II diabetes, being conceived for prolonged release of personalized doses of metformin in the upper gastrointestinal tract. With respect to other stomach-retentive devices already described in the scientific literature, the system here proposed comprised two different components: one responsible for retention into the target organ and the other one for controlled release of different doses of metformin, calculated to be compatible with the current needs of type II diabetes patients. Only upon assembly of these parts, the final GREDDS could be attained. This peculiar configuration allowed to take the most from the combined use of design, formulation and manufacturing strategies. Moreover, it made possible to deal with the system components individually and in parallel, thus simplifying and speeding up the experimental campaign while increasing the flexibility of the GREDDS under investigation. Indeed, any of the above mentioned parts might be fine-tuned independently and, in a wider perspective, be used for the development of other devices, following a lego-style assembly approach.

2. Materials and Methods

2.1 Materials

Metformin (d_{50} = 54 µm and d_{90} = 349 µm; Methapharmaceutical, ES); polycaprolactone (PCL; average Mw 14000, Sigma Aldrich, D); polyethylene glycol (PEG) 4000 (A.C.E.F., I); PEG 8000 (Clariant, I); polyethylene oxide (PEO; Sentry Polyox WSR N10 LEO NF, Colorcon, UK); polyurethane-based (TPU) filaments (nominal diameter 1.75 mm) (Flexmark 7, 8 and 9 identified as TPU 7, TPU 8 and TPU 9; TreeD Filaments, I); poly-lactic acid (PLA) filament (TreeD filaments, I);

hard-gelatin capsules DB caps size AAel (capacity 0.97 mL, internal body diameter 9.39 ± 0.06 mm, body length 19.05 ± 0.46 mm, overall closed length 22.6 ± 0.03 mm) and size 00el (capacity 1.02 mL, external body diameter 8.18 mm, body length 22.20 ± 0.46 mm, overall closed length 25.3 ± 0.03 mm) (Capsugel, I); silicon RPRO 30 base A and hardener B (Reschimica, I).

2.2. Methods

2.2.1 Manufacturing

3D printing by fused deposition modeling (FDM) was employed for manufacturing GREDDS components and testing samples (*i.e.* placebo cores and dumbbell specimens) to be used for either screening or development purposes, as described in the Results and Discussion Section. FDM was carried out by means of a Kloner3D 240 twin printer (Kloner3D, I) equipped with 0.5 mm nozzles. PLA and TPU 7, 8 and 9 filaments were printed as received. The main operating conditions set to 3D print different filaments are reported in Table 1.

Silicon-casting was employed for the fabrication of negative molds. These were composed of two halves and were subsequently used to melt-cast drug-containing cores starting from the formulations reported in Table 2. A previously weighed (Analytical balance, Gibertini, I) mass of drug and excipients were mixed in a mortar following the method of progressive dilutions and heated in a beaker up to 110 °C, under continuous mixing. The resulting molten formulations were poured into the silicon molds, which were then closed with manual clamps. After 30 min cooling at room temperature, the resulting drug-containing cores were manually removed from the molds.

All the specimens were characterized for weight (n = 6; Analytical balance, Gibertini, I), dimensions (n =6; MiniTest FH7200 equipped with FH4 probe, ø sphere = 1.5 mm, ElektroPhysik, D; caliper Mitutoyo, J) and were also photographed (V4K Ultra High Definition USB Document Camera, IPEVO, US-CA; GoPro Hero Session, US-CA; Optical microscope 5X magnification, Olympus BX 60, J). These data were used to evaluate, in an indirect way, the reproducibility of the manufacturing processes employed.

2.2.2 Characterization

DSC analyses were performed by a DSC Q100 (TA Instruments, US-DE), using nitrogen as a purge gas (70 mL/min). Indium was employed as a calibration standard. Samples of about 10 mg underwent 3 subsequent heating/cooling cycles from 0 °C to 250 °C (rate 10 °C/min).

SEM microphotographs were acquired by a Phenom XL SEM (Thermo Scientific, US-MA). Images of the top of the cores and of their cross-section (attained by cutting the samples on a plane perpendicular to the core axis) were taken.

Tensile tests (n = 3) were carried out on TPU filaments (gauge length L_0 = 25 mm) and on dumbbell specimens (L_0 = 27.5 mm) immediately after production, after drying or after being immersed for 15 days either in water or in HCl 0.1 N. During immersion, samples were checked for weight (Analytical balance, Gibertini, I) at pre-determined times. Independently of the treatment undergone, specimens were kept at a constant temperature of 23 °C prior to perform any mechanical characterization. Before testing, dimensions of the different prototypes were assessed (micrometer IP65 0-25 mm Mitutoyo, J). More into detail, diameter of the filaments was measured at 3 different points along their length, while thickness and width of the cross-section of dumbbell prototypes were evaluated at 3 points along their gauge length. Out of the measurements an average cross-section area (A_0) was calculated. The experiments were performed at strain rates of 0.0017, 0.017 and 0.17 s^{-1}. Since specimen slippage was unavoidable, results were considered valid up to a 300% sample deformation. In all cases, pneumatic grips closing at a pressure of 3 $\frac{kgf}{cm^2}$ were employed to reduce slippage, which especially occurred at the highest stretch level. From the measured force (F) and displacement (ΔL), nominal stress (σ) and nominal strain (ε) were calculated as follows:

$$\sigma = \frac{F}{A_0} \qquad \text{Eq. 1}$$

$$\varepsilon = \frac{\Delta L}{L_0} \qquad \text{Eq. 2}$$

Results were represented as stress *versus* strain curves.

Two different dynamometers were employed for tensile testing: *i)* a Hounsfield Dynamometer (Hounsfield, UK), equipped with a mechanical extensometer and a 5 kN load cell and *ii)* an Instron 5697 dynamometer (Instron, US-MA) provided with a 10 kN load cell. In the latter case, a non-contact method based on a video-extensometer system was employed to measure sample deformation. To this end, 5 lines (5 mm distant from each other) were drawn on the specimen and their motion was recorded with a 10M pixel camera (UI 5490 SE uEye, D). The resulting movie was divided into frames, which were processed by a specific image analysis software (ImageJ US-CA) to determine the local displacement (ΔL).

Besides the tensile characterization, cyclic tests entailing loading and unloading stages were performed on TPU filaments, using the Instron dynamometer equipped with the video-extensometer system. The cycle consisted in a stretching phase (up to 200% deformation) followed by unloading and was repeated at least 3 consecutive times on the same specimen. Loading/unloading phases were carried out either at a constant strain rate of 0.17 s^{-1}, or by setting a strain rate of 0.17 s^{-1} for loading and 0.017 s^{-1} for unloading.

Stress relaxation experiments required that a static tensile strain (ε_0) was quasi-instantaneously applied to the sample and maintained constant while measuring the stress (σ) evolution over time. These analyses were performed by means of the RSA3 Dynamic Mechanical Analyzer (TA Instrument, US-DE). Nominal tensile strains (ε_0) equal to 1, 2, 3, 4, 5 and 10% were applied to TPU filaments (L_0 = 12.5 mm). The experiments were carried out at several constant temperatures (*i.e.* from 25°C to 75 °C with 10 °C temperature steps,) and at $\varepsilon_0$values equal to 5 and 10%. From the measurements collected, the time evolution of the relaxation modulus, $E(\varepsilon_0,t)$, was determined as:

$$E(\varepsilon_0,t) = \frac{\sigma(t)}{\varepsilon_0} \qquad \text{Eq. 3}$$

By relying on the time-temperature reduction scheme, values measured at different temperatures and at $\varepsilon_0 = 10\%$ were superimposed to build a master curve for the relaxation modulus at the reference

temperature T_0 = 25 °C [71]. The application of the reduction scheme allowed to determine a shift factor ($a_T^{T_0}$) defined as follows:

$$a_T^{25} = \frac{t}{t^*} \qquad \text{Eq. 4}$$

where t and t* represent the time at which the relaxation modulus assumed the same value at a generic temperature T and at 25 °C, respectively. This quantity allowed for estimating the temperature effect in speeding up the viscoelastic time-dependent phenomena, and was particularly useful for designing accelerated testing procedures.

Funnel tests were performed (n = 3) using an experimental set-up adapted from the literature [24,27]. The RSA3 Dynamic Mechanical Analyzer was operated in compression-mode to force a prototype of the GREDDS under development into a funnel (45° angle, cylindrical opening of 20 mm in diameter) connected to the lower plate of the instrument (Figure 1). Both umbrella-like skeletons as such and assembled with PCL-based cores were evaluated. In the latter case, the specimen was positioned so that the core was oriented either in the advancing direction (*i.e.* named as the down position) or in the opposite one (*i.e.* named as the up position), as sketched in Figure 1. Moreover, umbrella-like skeletons were tested *i)* immediately after manufacturing, *ii)* after 4 hours upon insertion into hard-gelatin capsules, to resemble extemporaneous preparation of the system to be administered, and *iii)* following storage at 55 °C for pre-defined time periods, thus accelerating any changes that might occur after-long term storage at room temperature.

The sample under evaluation was manually positioned at the center of the funnel, in contact with its wall, and pushed down at a constant rate of 0.1 mm/s for 250 s, while measuring the forces it opposed to the movement of the piston. The data collected were represented as force *versus* displacement curves. Here different zones can be recognized: *i)* at low displacements (*i.e.* up to about 12 mm), the arms of the umbrella-like skeleton slip against the converging surface of the funnel, reaching the limit of its narrow zone, *ii)* the arms stopped at that position, while the connection ring was pushed into the narrow section, *iii)* the peak force was reached and the arms folded as well as entered the narrow

section of the funnel, sliding along the almost vertical wall of the latter. Out of the observed motion/deformation mechanism and based on previous literature data, the maximum force required for samples to pass through the funnel represented the ability of the system to resist gastric contractions and was used to compare different samples.

Opening tests were performed on prototypes (n = 6) folded into hard-gelatin capsules. These were immersed into a 250 mL crystallizer filled with 200 mL of HCl 0.1 N and kept at 37 °C. Their behavior upon contact with the media was recorded using a camera (UI1490LE-M-GL Ueye camera, IDS imaging, D; Computar MACRO 10×, lenses, J) and monitored with a stopwatch (digital stopwatch, Wokex, I). From the recording, the opening time of the capsules as well as the deployment time of the folded prototypes here contained were determined. In order to estimate the degree of recovery of the initial unfolded geometry, specimens were photographed from above before and after the experiment (V4K Ultra High Definition USB Document Camera, IPEVO, US-CA). Image J software was employed to measure, on the images acquired, the diameter of the circumference surrounding the projection of the umbrella-like skeleton on the observation plane (Figure 2). The closer the radius of the unfolded prototype was to its original value before folding, the closer its shape would be to the original planar one.

Samples were tested immediately after manufacturing and upon storage of the umbrella-like skeleton at 55 °C for increasing times (up to 18 h depending on the TPU grade) that corresponded to 18 months' storage at room temperature, according to the time-temperature reduction scheme.

Mass-loss tests were performed on PCL-based drug containing cores (n = 3). These were kept at 25 °C in unstirred conditions, using NaOH 5 M (pH = 14) as the aqueous medium to accelerate polymer degradation, as already reported in the literature [72-74]. Samples were immersed into 20 mL of this solution and withdrawn at pre-determined time-points (*i.e.* 0.5, 1, 3, 6, 24, 48, 72 h and 5 as well as 7 days). After removal, they were washed 3 times with distilled water and let to dry for 8 h at 40 °C (WVR oven, I). Once completely dry, the specimens were checked for weight (Analytical balance, Gibertini, I) and the percentage of mass loss (m_l) was calculated as:

$$m_l(\%) = \frac{m_d - m_0}{m_0} \times 100 \qquad \text{Eq. 5}$$

where m_d and m_0 represent the mass of the sample after drying and before starting the experiment, respectively.

Release tests were carried out on PCL-based drug containing cores either alone or inserted into umbrella-like skeletons (n = 3), using a USP38 dissolution apparatus 2 (800 mL HCl 0.1 N, kept at 37 ± 0.5 °C; 50 rpm) (Distek, CH). Fluid samples were withdrawn at specific time points and assayed spectrophotometrically (λ = 237 nm). The drug concentrations were determined using a calibration curve purposely built in the 0.01 - 1 mg/mL range (R^2 = 1.000). In addition, the release data obtained were analyzed using the Korsmeyer-Peppas model:

$$\frac{M_t}{M_\infty} = K \cdot t^n \qquad \text{Eq. 6}$$

where $\frac{M_t}{M_\infty}$ represents the fraction of drug released at time t, while K is the kinetic constant (dimension of time^{-n}) and n the diffusional exponent (dimensionless). Both K and n depend on structural and geometric characteristics of the system. Data were fitted up to $\frac{M_t}{M_\infty} = 0.6$

3. Results and Discussion

3.1 Design concept

The main features envisaged for the new GREDDS to be developed were:

- simplicity of administration and operation, as well as ease of disposal once exhausted, which would increase patient compliance and safety;
- sufficiently prolonged retention within the stomach and controlled release;
- flexibility in terms of metformin dosing and release rate, to meet different therapeutic needs of subjects suffering from type II diabetes.

To fulfill the above mentioned requirements, the system was designed to be composed of: a central core and an umbrella-like skeleton entailing 5 arms joined together, responsible for drug release and

retention performance, respectively. The choice of decoupling the release-controlling part from that ensuring retention was quite new in the field and was intended to increase the versatility of the system. This way, the key aspects of each component could be assessed independently and in parallel, thus making the research efforts more effective.

The core entailed a hemispherical-shaped end, purposely designed to fit the body of a commercially available capsule and to act as the respective cap. This choice allowed not only to have the final system resemble the shape of a capsule, being more acceptable from the patients' perspective, but also to maximize the volume of the core so as the strength of metformin that could be loaded. Indeed, the drug quantity conveyed in this system was intended to fulfill the actual therapeutic needs of subjects suffering from type II diabetes.

By inserting the core, from its smaller end, into the central ring of the umbrella-like skeleton, the two parts were assembled in an expanded configuration, suitable for retention of the system into the stomach. By folding the arms of the umbrella-like skeleton against the core, a collapsed shape was attained, which was able to fit within the body of the selected capsule. This way, locking and oral administration of the assembled DDS would be possible. In Figure 3, final electronic models of the various components of the GREDDS, either as such or upon assembly, are reported together with photographs of the actual prototypes.

Following the form-fit-function approach, the individual components of the GREDDS were designed by taking into account the characteristics necessary for proper interaction with each other and to guarantee effective working mechanism of the assembled device. It was therefore fundamental to identify, at an early stage of development, the key quality parameters for each part, taking into account how shape, dimensions and performance might differ from pre-determined values without impairing function. As a result, the selection of appropriate materials for the different components of the GREDDS played a pivotal role.

3.2 Core

3.2.1 Design

The core of the GREDDS was designed *i)* to convey personalized doses of metformin, in order to better address the need of specific diabetic patients, who might become less responsive to the drug over time, and *ii)* to release them in a controlled way. In addition, the amount of active ingredient contained needed to be compatible with, at least, one day of treatment. Indeed, as previously discussed, the current therapeutic regimen for type II diabetes entails the use of 500-1000 mg of metformin. The latter is administered multiple times through the day *via* IR tablets, leading to a drug bioavailability of approximately 50%. Better results could be attained by resorting to GREDDSs able to continuously release the selected active ingredient at the appropriate absorption site, thus reducing the chances of drug loss. This way, not only the overall dose of metformin taken daily could be reduced, but also the number of relevant administrations. As a result, a 500 mg dosage strength could become compatible with a 24-48 h treatment. For this reason, it was chosen as the first target for the GREDDS under investigation. However, such a high dose occupies a major volume, posing serious challenges for development of a prolonged-release matrix, which needs to be formulated with specific adjuvants to ensure the expected performance. Dimensions of AAel DB capsules were set at the highest limit for the system in its collapsed shape to maximize drug load as well as formulation space, while still ensuring easy swallowing of the DDS. This allowed for clear definition of overall length and diameter of the system, and also guided the design of the cap-shaped end of the drug containing core (Figure 3).

3.2.2 Manufacturing

The quite high drug load to be conveyed into the core along with the need for prolonged release steered the choice towards a high-density system to be produced by hot-processing starting from a

matrix-forming polymer capable to ensure controlled release over 24 h, even at low concentrations [75-79]. To this target, resorting to either inert or hydrophilic swellable/soluble polymers traditionally employed in the formulation of oral products did not seem appropriate. On the other hand, excipients typical of other administration routes and especially proposed for long-term applications were considered. In this respect, PCL was selected as an interesting matrix-forming polymer for a variety of reasons Besides having been tested for the manufacturing of prolonged-release inserts/implants, its biocompatibility, mechanical properties as well as biodegradability profile in physiological conditions (upon hydrolysis of their ester linkages) have already been deepened [80-85]. In addition, degradation and release rate from PCL-based matrices could be fine-tuned through the use of appropriate additives [25,86-88]. Focusing on core manufacturing, this polymer could easily undergo hot-processing, in view of its melting point of 60 °C as well as of a glass transition temperature of about -60 °C [89-91]. Finally, PCL potential outside the field of implantable systems has been recently demonstrated. Indeed, it was proposed for the fabrication of controlled-release DDSs to be orally administered, even resorting to novel manufacturing approaches (*e.g.* injection molding, 3D printing, electrospinning) [24,25,27, 92-95].

A relatively low molecular weight PCL (*i.e.* 14000 Da) was preferred for this study. Indeed, higher grades would imply excessively long degradation times, ranging from 3 weeks to 3 years, which would not be compatible with the 2 days treatment targeted for the GREDDS under development [96-98]. The PCL-based drug-containing cores were produced by melt-casting, which was easy to perform at lab-scale and allowed to contain the starting investments in manufacturing equipment. This strategy is fundamental during R&D stages of a new DDS, because the experiments are mainly aimed at attaining prototypes for preliminary validation studies. Therefore, melt-casting started to be employed by many researchers, with promising results also towards the possibility of using the data collected in subsequent scale-up phases, entailing for instance other hot-processing techniques more suitable for large-scale production (*e.g.* hot melt extrusion, injection molding) [27,99].

Very preliminary attempts towards the use of 3D printing for prototyping activities were poorly successful, probably due to the limited viscosity of the PCL-based melt. Indeed, the low viscosity was responsible for uncontrolled dripping of the material from the 3D printer nozzle and for unsuitable cooling, despite the tentative changes to modify retraction-associated parameters to control such a phenomenon. As a consequence, the first printed layers were not able to withstand the weight of the subsequent ones, as required when an object is built layer-by-layer. However, FDM was essential for printing PLA-based prototypes of the core and for fine-tuning their details. Indeed, such FDM prints were used as templates for the manufacturing of negative silicon-based molds, which were then employed in melt-casting of actual drug-containing cores.

A range of PCL-based formulations were prepared, not only for testing increased drug loads, but also for fine-tuning the performance of the core, by adding a variety of adjuvants at different concentrations. Polymers freely-soluble in water were selected because, due to their high hydrophilicity, were expected to enhance the degradation rate of the PCL-based samples and to speed up drug release. These included PEGs with diverse molecular weights and PEO, which is well-known to grow about 50% in volume prior to solubilization, thus having the potential to create major discontinuities into the PCL structure. As far as metformin is concerned, relevant HCl salt was selected because it is water soluble and has a melting point around 222-226 °C. As a consequence, it should remain suspended into the polymeric melt, as also confirmed by DSC (data not shown).

Despite the manual procedure for relevant manufacturing, all the melt-casted cores pointed out reproducible weight (1010 mg, CV ≤ 10%) and dimensions analogous to the nominal ones. To better appreciate the microstructure, SEM photomicrographs of the prototypes obtained were also acquired. By way of example, images relevant to samples of different composition, taken both on their external surface and on relevant cross-section, are collected in Figure 4.

As expected, the hot-processing technique employed resulted in all the specimens exhibiting a relatively compact structure, irrespective of their formulation. Indeed, a limited number of pores were visible, appearing as little dark holes into the grey polymeric matrix. No major differences were

highlighted when comparing different areas (*i.e.* outside versus inside). Moreover, metformin particles turned out clearly visible and homogeneously distributed inside the polymeric structure. Indeed, drug white crystals emerged on the external surface of the items, thus being immediately available for interaction with aqueous fluids. Interestingly, the number of such crystals seemed higher on the surface of the sample corresponding to the junction between the two halves of the mold. Although the prototypes appeared quite smooth when inspected visually, a certain surface roughness was noticed by looking at the SEM photomicrographs, which highlighted repetitions of small steps of material. This was consistent with the fabrication mode of PCL-based parts. Indeed, the cores were manufactured using silicon molds that were casted starting from previously printed PLA-based templates. Therefore, their layer-by-layer structure was first transferred to the mold and then to the molten material during melt-casting of the drug-containing samples.

3.2.3 Performance

Mass loss analysis of cores based on neat PCL and loaded with either 25 and 50% of metformin were first carried out (Figure 5a). Then PCL-based prototypes containing 50% of the drug and either 10 or 25% of soluble adjuvants instead of PCL were tested (Figure 5b). In particular, PEO was loaded at 10% only, due to the high viscosity and poor homogeneity of the resulting melt when dealing with higher concentrations. Based on the existing literature, the mass loss experiment involved the use of basic pH fluids to speed up PCL degradation and to better highlight the contribution of the different release modifiers [72-74]. This strategy was deemed particularly cost-effective, thus suitable for a feasibility study. In fact, resorting to the use of enzymes for the same purpose would have been more challenging, introducing major source of variabilities in the experimental set-up and thus in the associated outcomes. Indeed, type, concentration, extraction source and specific working conditions (*e.g.* pH, temperature) for each enzyme considered would have been crucial [100-101]. Moreover, the scientific literature indicated that the effect of efficient enzymes towards PCL degradation (*e.g.* lipases) would start to be relevant after a relatively long interaction time [100,102,105]. By way of

example, it is reported that lipases can degrade PCL to oligomers and monomers within 3-4 weeks, while in normal conditions no degradation would be visible for 9 weeks [80,101,106-108]. Based on these considerations, the use of enzyme-containing media could be expected to have a major impact on the final elimination of the exhausted GREDDS and was avoided for assessing the release performance at this stage because, for our system, the latter was planned to correspond to only a few days of treatment.

While the weight of neat PCL-based prototypes remained practically unchanged over 7 days (mass loss < 0.8%), samples containing 50% of metformin loose approximately half of their initial weight after 2 days of testing. The rate of mass loss increased over time, probably due to a rise in the surface area of PCL exposed to degradation (*i.e.* cleavage of the polymer ester linkages), which was caused by the dissolution of the soluble drug. Indeed, by remaining suspended into the polymeric matrix, the metformin particles acted as pore formers.

Focusing on the behavior of specimens containing soluble adjuvants, mass loss turned out even faster, in agreement with preliminarily literature findings in this respect [25,86-88,109-112]. More into detail, mass loss data increased in the PEO > PEG8000 > PEG4000 order. The higher the amount of excipient added, so as the lower the PCL content, the higher the rate of mass loss. Interestingly, the action of PEO turned out visible after 2 days, probably because relevant swelling needed a certain time to become effective.

Consistent results in terms of release rate were observed for metformin-containing PCL cores. In this case, *in vitro* testing took place in enzyme-free acidic media according to targeted biological environment (Figure 6). As expected, a particularly slow release, even exceeding the desired time-frame of 2 days, was pointed out by cores based on neat PCL. More into detail, the lowest release rate was observed with samples having the highest polymer content, so as the lowest drug dose (*i.e.* 25%). Indeed, they lasted for about 14 days. On the other hand, release duration was reduced to 6 days when dealing with cores containing 50% of metformin, which was further proven to act as a soluble pore-former. Overall, drug delivery turned out faster when the PCL content within the matrix

was decreased. Moreover, the possibility of fine-tuning the system performance according to the characteristics and the amount of the adjuvant employed was demonstrated.

The release data collected were also analyzed using the Korsmeyer-Peppas model, which is widely employed for describing drug release from polymeric systems and has been recently applied to deepen the performance of PCL-based matrices [113-116]. Indeed, this power law was demonstrated useful when the release mechanism is unknown or when more than one phenomenon would occur concomitantly (*e.g.* diffusion of water into the matrix as well as swelling and dissolution of the latter). The values of the n exponent, well-known for providing information on the drug release mechanism (*i.e.* Fickian diffusion *versus* non-Fickian one), were calculated for all the drug-containing cores under evaluation and are summarized in Table 3. Cores made with PCL and containing 50% metformin were the only characterized by n value of 0.500 and a narrow 95%-confidence-interval, thus indicating a diffusion-controlled release mechanism. The behavior of samples of analogous composition but with reduced drug content (*i.e.* 25% of metformin) was quite similar (n = 0.514). Conversely, all the other prototypes clearly exhibited a non-Fickian diffusion mechanism (*i.e.* $0.5 < n < 1$). Interestingly, although specimens containing 50% of the selected drug combined with 25% of different PEGs pointed out mean n values closer to 0.5, their 95% confidence interval turned out very wide.

After 6 months' storage (25 ± 5 °C, 55 ± 5 % RH), drug-containing cores were further tested for release. The resulting profiles turned out analogous to those previously discussed, which was deemed particularly promising towards stability of the DDS under investigation.

Overall, the data collected supported the feasibility and the application potential of the drug-containing core of the novel GREDDS under development. More into detail, interesting relations among size, shape, composition (*i.e.* type and amount of adjuvants as well as strength of metformin conveyed) of this part and relevant degradation as well as release performance were highlighted. In a further development step, this preliminary information will necessarily be supplemented and supported by data on stability and safety of use in the physiological environment.

3.3 Umbrella-like skeleton

3.3.1 Design

In the actual configuration of the GREDDS, the umbrella-like skeleton was responsible for the attainment of collapsed and expanded shapes, ensuring administration and retention, respectively. To this aim, it was conceived as a set of flexible arms joined through a central ring (Figure 3). The latter would not only connect the above-mentioned arms and enable folding and unfolding, but also ensure proper assembly of the final system, allowing for correct positioning of the core. In addition, the dimensions of the arms were such that, upon folding, they would completely fill the space left by the core in the capsule body.

The expanded configuration of the umbrella-like skeleton was designed to be inscribed within a circumference of 35.7 mm in diameter. This choice was made to avoid passage of the umbrella-like skeleton in the expanded configuration through the open pylorus. Indeed, when open, the diameter of such sphincter could reach 22.1 mm but more commonly is reported to be in the 13-17 mm range [17,29]. Focusing on the arms, two different thicknesses were initially considered (*i.e.* 1 and 2 mm), to evaluate the influence of this parameter on the umbrella-like skeleton behavior. Notably, the dimensions of the skeleton arms could impact on the encumbrance of the device when in the folded configuration, but these thicknesses were selected because they did not impair the possibility for the system to be housed in commercially-available capsule bodies. Besides size requirements, the mechanical behavior of this component was fundamental for the final performance of the GREDDS, as it should be able to fulfill many different needs. As long as the GREDDS would remain into the stomach, it should resist gastric contractions while maintaining its cumbersome shape and without representing a potential hazard for the physiological environment. From the administration point of view, the collapsed configuration had *i)* to be easily achieved by folding the arms without breaking or damaging them and *ii)* to be maintained inside the body of a standard capsule over the product

shelf-life. At any time during this period, upon administration of the GREDDS, the arms were expected to undergo an immediate elastic deployment following capsule dissolution in the stomach environment. Even if the unfolding process of the umbrella-like skeleton does not occur instantaneously, it should take place fast enough to ensure the recovery of a sufficient fraction of its initial diameter, thus preventing early elimination of the system from the open pylorus. Such folding/unfolding requirements imply that the material behavior should be elastic up to high deformations (*i.e.* hyperelastic) or, at most, viscoelastic with a relatively low relaxation time. In this respect, no or very limited permanent deformations should result from the folding phase.

3.3.2 Manufacturing

Considering the peculiar deployment performance envisaged for the umbrella-like skeleton, excipients commonly employed in the manufacturing of DDSs would not guarantee its correct functioning. Therefore, the research of a compliant material was broadened to the medical device field, in order to include thermoplastic elastomers composed of soft and hard segment. Among those, TPU was deemed as particularly promising in view of its hyperelastic (*i.e.* non-linear elastic) mechanical response and stability in a variety of challenging environments (*i.e.* extreme pH values, various solvents, different temperature conditions) [117-120]. In addition, preliminary research findings suggested the suitability of this material for pharmaceutical applications and particularly for the formulation of DDSs intended for oral administration [24,27,121-129]. As a further advantage, filaments based on TPUs with different mechanical characteristics are already available, favoring the use of FDM for manufacturing the umbrella-like skeleton. This technique was deemed interesting due to its capability to deliver complex shapes and to ensure their modification in real-time [75,130-132].

The FDM process required a range of preliminary trials to identify the best conditions for printing this GREDDS component. First, TPUs with different nominal hardness (*i.e.* ranging from a very soft 70 Shore A of TPU 7 to a relatively hard 95 Shore A of TPU 9) were selected. Since their viscosity

remained particularly low at the appropriate processing temperature, speed and retraction distance were set to high values to avoid early flow of the material from the nozzle. Indeed, the latter resulted in the so-called stringing effect, which occurred when the printer-head oozed some melted polymer during its travel across an open space to reach the next point. When these strings solidified, they resembled a cobweb, affecting the appearance and the performance of the final item. Not only was the printing speed maintained low, but also the motion of the printer-head was enhanced by manually acting on the G-code to reduce undesired travels across the part under construction and relevant distances, thus resulting in a reduced fabrication time. Moreover, as the different arms of the umbrella-like skeleton needed to be considered as a single part, their G-code was modified accordingly. In particular, the angle of the infill was adjusted to have it always oriented in the axial direction of the arm (*i.e.* the radial direction of the circle circumscribing the umbrella-like skeleton). In other words, the infill pattern resembled spokes of a wheel surrounding the central ring. This strategy was pursued to have all the arms printed (thus in principle behave) in the same way and to increase their resistance towards any tractions they might undergo during their folding in the collapsed shape. For the same purpose, the perimeters of each arm and those of the central ring were not just partially superimposed, as happened in standard printing settings, but were completely overlapped to ensure a strong anchoring. Indeed, quality and reproducibility of the common area between the arms and the ring walls was the most critical to be controlled. Moreover, for correct folding and unfolding of the umbrella-like skeleton, a solid connection between these zones was required, as they would receive the most stress.

By identifying appropriate 3D printing conditions, the resulting prototypes pointed out good weight reproducibility (240 mg, CV $\leq$ 5% and 460 mg, CV $\leq$ 4% for system having 1 and 2 mm thick arms, respectively) and dimensions analogous to the nominal ones even in the most challenging areas, *i.e.* arms (CV $\leq$ 10%).

Aiming at predicting the mechanical performance of the umbrella arms, a preliminary investigation was performed, focusing on the thermo-mechanical behavior of TPUs characterized by different

nominal hardness. The experimental campaign started from uniaxial tensile experiments carried out on filaments. As the thermo-mechanical history applied to the polymer during 3D printing may affect the properties of the final item, printed dumbbell specimens were also tested. These samples represent the geometry of choice for preliminary trials and, being relatively easy to fabricate, they were 3D printed in conditions similar to those used for the umbrella-like skeleton. In Figure 7, the results of tensile tests attained from filaments and 3D printed dumbbells are summarized. As expected, TPU 9 always had a stiffer behavior than TPU 8 and 7 (Figure 7b). However, major differences were observed between filaments and printed specimens, which may be ascribed either to a different material behavior upon processing or to a misestimation of the effective area of the samples. To separate these two effects, dumbbell specimens were cut, observing their cross-section with an optical microscope. As visible from the photograph reported in Figure 7a, the presence of pores/discontinuities was highlighted and these could markedly reduce the resistant surface with respect to the nominal one. Therefore, an effective cross-section area was calculated for all the printed samples and used to correct the tensile tests data. The stress-strain curve following this adjustment correlated very well with those relevant to TPU 7 and 8 filaments, confirming that the printing process did not affect the properties of the starting material. As for TPU 9, a slight effect of processing could not be excluded. Indeed, at relatively high strain levels, the corrected curves relevant to dumbbell specimens did not perfectly overlap to those of filaments. Overall, 3D printing seemed to have only a small effect on the selected TPUs, which allowed for further investigation of the material behavior using just filaments as screening samples.

Stress-strain curves resulting from tensile tests performed at different strain rates (*i.e.* 0.0017, 0.017 and 0.17 s^{-1}) and from samples immersed either in distilled water or in HCl 0.1 N are reported in Figure 8a and 8b, respectively. The former conditions allowed for estimating the viscoelastic behavior (here intended as strain rate dependence) of the different TPU grades considered, which turned out negligible for TPU 7 and limited for TPU 8 and 9. On the other hand, exposure to different aqueous media, even for relatively long times, did not markedly affect the response of any TPUs, which might

be especially promising considering the targeted application. Overall, the data pointed out good reproducibility, especially at lower ε values.

In order to gather information regarding the suitability of the TPUs under investigation for 3D printing umbrella-like skeletons, two aspects were mainly investigated: *i)* the ability of TPU filaments to recover the applied strain in cyclic tests, which would highlight any possible non-recoverable bending, and *ii)* their stress relaxation over time at fixed deformation. This would occur when maintaining the system within a capsule for relatively long times and would provide an indication of the rate of the subsequent unfolding.

Focusing on the results of loading-unloading tests, a residual strain of limited entity was observed after a first cycle carried out up to 200% (Figure 9a). Such a residual strain increased with stiffness of the considered TPU. After this first cycle, the residual strain did not present any major changes. From the second cycle on, all the materials showed a lower value of stress at the same strain with respect to what previously highlighted. This suggest that the unfolding might be incomplete and that the ability of the umbrella-like skeleton to sustain loads during gastric contractions could be reduced after repeated folding/unfolding.

To better understand stability of the umbrella-like skeleton, intended as the impact of maintaining this part folded within a capsule for relatively long times, a viscoelastic characterization was deemed fundamental. Indeed, deployment of the skeleton should take place even after a prolonged storage, during which the system will be subjected to an imposed constant strain. In this respect, the stress relaxation phenomena might affect its unfolding performance upon removal of the external constraint represented by the capsule body. When tested at different strains (*i.e.* 1, 2, 3, 4, 5 and 10%), the relaxation modulus of all the TPU filaments considered decreased monotonously with respect to the applied strain. By way of example, data relevant to samples tested at 25 °C are reported in Figure 9b. As expected, the relaxation modulus determined in fixed time and applied strain conditions increased with the TPU hardness. Moreover, for each TPU grade investigated, the relaxation modulus at fixed time decreased by applying higher strain, indicating a non-linear viscoelastic behavior in a

deformation range of interest for the umbrella-like skeleton. Finally, the relaxation occurred faster for TPU 9 and could not be disregarded for any TPUs. To speed up the-above mentioned phenomenon, the investigation was deepened by taking into account different temperatures. In these experiments, only the most severe strain (*i.e.* equal to 10%) was applied. Relying on the time-temperature reduction scheme and shifting the results along the logarithmic time axis, the relaxation modulus master curve was built (Figure 9c). The trend of the latter not only confirmed that TPU 9 relaxed faster than TPU 8 and 7, but also highlighted a certain stress relaxation. This has to be accounted when considering the possible effects of long-term storage of the umbrella-like skeleton within a capsule. To this end, stress relaxation of folded samples was accelerated by conditioning them at 55 °C for 56, 99 and 314 min for TPU 7, 8 and 9. These times were calculated based on the time-temperature reduction scheme to be representative of 18 months' storage at 25 °C, thus allowing to preliminary assess the stability of the system over time.

3.3.3 Performance

The unfolding capability of the TPU component of the GREDDS under development needed to be evaluated, as it would be responsible for the gastric retention ability of the entire system. In this respect, unfolding rate and efficiency of umbrella-like skeletons with arms of different thickness were assessed by measuring: *i)* the time needed for complete deployment following contact with HCl 0.1 N, and *ii)* their ability to regain the initial diameter. In this respect, samples were tested either immediately after folding and insertion within a capsule, or following storage under the accelerated conditions previously defined (corresponding to 18 months' storage at ambient conditions) (Figure 10). For simplicity reasons, experiments were performed on umbrella-like skeletons without the drug-containing cores, after having verified that the presence of the latter did not affect the unfolding mechanism. The specimens tested immediately after insertion into the capsules showed the desired deployment, regardless of the arm thickness. Indeed, they reached dimensions similar to those measured before folding (diameter of 36.00 ± 1.02 mm and 35.96 ± 1.22 mm for skeletons provided

with 1- and 2-mm thick arms, respectively) (Figure 10a and 10a'). In terms of kinetics, all the TPU-based specimens did not unfold instantaneously. However, the deployment time was always lower than 70 s from the capsule opening (Figure 10b and 10b'). Since this value was lower than the time required for capsule dissolution (74-98 s), it was deemed acceptable. More into detail, unfolding times decreased with increasing TPU modulus. This may be explained by an active action of the arms. Indeed, the latter probably fostered the opening of the capsule by breaking and moving apart its walls, with the action of stiffer arms being more effective. Focusing on the storage impact, a small tendency towards a reduction in the dimensions of the deployed umbrella-like skeleton was observed and resulted less evident for samples provided with 2 mm thick arms. Nevertheless, the diameter values attained were always greater than those reported for the open pylorus, thus in principle not affecting the retention performance of the samples. With respect to the opening time, it generally increased with storage, with no major differences between umbrella-like skeletons having 1 or 2 mm thick arms. Further information on the functionality of the umbrella-like skeleton were gathered taking advantage of the funnel test. According to the literature, this experiment would provide the maximum resistance a GRDDS would oppose to forces that are expected to push it through a predefined rigid funnel restriction, intended to roughly mimicking the gastric sphincter [24,27]. Indeed, data already published suggested that only systems capable of withstanding forces from 1.9 to 3 N might be compatible with gastric retention [24,133]. The funnel experiment was thus carried out on assembled systems (*i.e.* PCL-based cores inserted into the TPU-based umbrella-like skeletons). The latter were either conveyed in a capsule for a limited period (identified as t = 0 s), thus accounting for the time needed for the extemporaneous preparation of the GREDDS before relevant administration, or upon storage (Figure 11). This was done to preliminarily estimate stability of the system response over time. As before described, storage was performed by keeping the umbrella-like skeletons at 55 °C for a certain time, which was calculated to be equivalent to 18 months' storage at 25 °C (t_{eq} = 18 months). Since previous tests highlighted a reduction in force at fixed deformation after a loading-unloading cycle, folding was also performed immediately after manufacturing. The experiments were repeated

on assembled systems differing for the position of the hemispherical-shaped end of the core while passing through the funnel (see Figure 1). Indeed, it would not possible to predict the direction in which the system would approach the pylorus *in vivo*.

The results of the funnel tests underlined that the higher the modulus of the TPU used for printing the umbrella-like skeleton, the higher the force required to push it. Moreover, the force data turned out greater when dealing with samples in the up position. Indeed, in such position, the top part of the core acted as a physical obstacle, thus hindering undesired folding of the TPU-based arms. However, prototypes having 1 mm thick arms reached, in the best case scenario (*i.e.* umbrella-like skeletons based on TPU 9 and tested in the up position), peak values of about 0.5 N only. Alternatively, for samples entailing arms of 2 mm in thickness, force peaks up to 4 N were registered, thanks to an increased arm stiffness through the rise of its momentum of inertia. Specimens tested after storage always pointed out lower force data. This behavior could be associated with a limited recovery of the unfolded shape upon long-term maintenance within the capsule. Indeed, these umbrella-like skeletons were characterized by a truncated cone shape, which made expulsion from the funnel easier, especially when they were tested in the down position.

3.4 Ongoing work

Based on the data collected so far, preliminary trials were performed on assembled systems (*i.e.* having the drug-containing core inserted into the umbrella-like skeleton, with the latter folded and conveyed within a commercially available capsule body). As expected, not only was the opening performance of the GREDDS prototypes analogous to that observed with screening samples, but also their release profiles were superimposed to those attained when dealing with the cores alone. Funnel tests were also carried out on assembled devices subjected to release experiments. Samples were withdrawn at specific time points and tested, in order to rule out possible impact of contact with the acidic media over time. Interestingly, the maximum forces attained turned out comparable to the values previously discussed. Only when the PCL-based cores were exhausted and completely

degraded, the maximum forces required to push the umbrella-like skeletons out of the funnel were markedly reduced (≤ 0.3 N). This result was considered particularly promising towards possible spontaneous elimination of the system from the stomach at the end release.

The overall behavior pointed out by assembled prototypes supported the suitability of the approach followed in this work, *i.e.* dealing with individual components of the device in parallel for simplifying and speeding up further experiments.

3.5 Future perspectives

The present study was intended to be part of a wider work, in the perspective of which the feasibility evaluation here described represented the first step. Indeed, the relations found between material properties, composition and performance of each component of the GREDDS under investigation were preparatory for further experiments and intended to guide the next research steps. These will be mainly aimed at increasing the resistance of the umbrella-like skeleton towards the funnel experiments, for instance *i)* fine-tuning the dimensional details of this component by means of a rational design process, and *ii)* identifying alternative materials for its manufacturing (*e.g.* different grades of thermoplastic polyurethanes or other thermoplastic elastomers). At the same time, the formulation of the drug-containing core will be optimized to perfectly match the expected 2 days-lasting release. Finally, great attention will be paid at finding novel design/composition strategies that will favor removal of the system from the stomach when required. By way of example, a new configuration of the umbrella like-skeleton is currently under evaluation, involving the presence of segments that could be degraded in the gastric environment. This is expected to occur only after complete release of metformin from the core, which would make the exhausted GREDDS smaller than the pylorus, thus favoring its spontaneous elimination from the gastrointestinal tract. In parallel, the resulting prototypes will be deeply assessed for safety and reproducibility of their overall performance, for instance planning *in vitro* tests relying on the use of simulating gastric fluids differing for type and quantity of enzymes, as well as *ex vivo* and *in vivo* experiments.

4. Conclusions

Following a renovated interest for GRDDSs, especially in view of the suitability of such systems for therapy personalization and the possibility of using innovative technologies and materials for their manufacturing, a novel metformin-containing expandable device for the treatment of type II diabetes was designed and its feasibility was preliminarily demonstrated. The system proposed was intended to guarantee prolonged release of the drug at its absorption window, in order to cover one or more days of treatment with a single oral administration. It was conceived to include a drug-containing core based on PCL, ensuring controlled release, and a TPU umbrella-like skeleton. The latter was responsible for the achievement of the collapsed shape for oral intake and of the expanded one for gastric retention. Each of these parts was thoroughly characterized for key quality parameters: thermo-mechanical properties, resistance to simulated gastric contractions, stability, interaction with aqueous fluids, release as well as folding/unfolding performance. Thanks to the work performed, important links have been identified between composition and size/shape of each of the above mentioned components, which supported the feasibility and will be fundamental in the development of the final GREDDS.

The authors have no other relevant affiliations or financial involvement with any organization or entity with a financial interest in or financial conflict with the subject matter or materials discussed in the manuscript apart from those disclosed.

This paper was not funded.

References

1. Lopes CM, Bettencourt C, Rossi A, et al. Overview on gastroretentive drug delivery systems for improving drug bioavailability. Int J Pharm. 2016;510(1):144-158.
2. Kumar M, Kaushik D. An overview on various approaches and recent patents on gastroretentive drug delivery systems. Recent Pat Drug Deliv Formul. 2018;12(2):84-92.
3. Pinto JF. Site-specific drug delivery systems within the gastro-intestinal tract: from the mouth to the colon. Int J Pharm. 2010;395(1-2):44-52.
4. Streubel A, Siepmann J, Bodmeier R. Gastroretentive drug delivery systems. Expert Opin Drug Deliv. 2006;3(2):217-233.
5. Baride KS, Chemate SZ, Borkar GS, Patil GB., An overview of the gastroretentive drug delivery system, Int. J. Pharm. Sci. Rev. Res. 2023,80(2):104-115
6. Uboldi M, Melocchi A, Moutaharrik S, et al. Administration strategies and smart devices for drug release in specific sites of the upper GI tract. J Control Release. 2022;348:537-552.
7. Awasthi R, Kulkarni GT. Decades of research in drug targeting to the upper gastrointestinal tract using gastroretention technologies: where do we stand?, Drug Deliv. 2016;23(2):378-394.
8. Dhiman S, Philip N, Singh TG, et al. An insight on novel approaches & perspectives for gastro-retentive drug delivery systems. Current Drug Deliv. 2023;20(6):708-729.
9. Melocchi A, Uboldi M, Cerea M, et al. A Graphical review on the escalation of fused deposition modeling (FDM) 3D printing in the pharmaceutical field. J Pharm Sci. 2020;109(10):2943-2957.
10. Tripathi J, Thapa P, Maharjan R, et al. Current state and future perspectives on gastroretentive drug delivery systems. Pharmaceutics. 2019;11(4):193.
11. Vrettos NN, Roberts CJ, Zhu Z. Gastroretentive technologies in tandem with controlled-release strategies: A potent answer to oral drug bioavailability and patient compliance implications. Pharmaceutics. 2021;13(10):1591.

12. Pal R, Pandey P, Nogai L, Arushi, Anand A, Suthar P, Keskar MS, Kumar V., The future perspectives and novel approach on gastro retentive drug delivery system (GRDDS) with currrent state. J. Popul. Ther. Clin. Pharmacol. 2023;30(17):594-613

13. Sambre TK, Mehta T, Sambre TT, Saga of gastroretentive drug delivery system: emerging concepts, recent advances and technological progress, Int. J. Pharm. Sci. Res. 2023;14(5):2030-2059

14. Abramson A, Caffarel-Salvador E, Khang M, et al. An ingestible self-orienting system for oral delivery of macromolecules. Science. 2019;363(6427):611-615.

15. Abramson A, Frederiksen MR, Vegge A, et al. Oral delivery of systemic monoclonal antibodies, peptides and small molecules using gastric auto-injectors. Nat Biotechnol. 2021;40(1):103-109.

16. Abramson A, Kirtane AR, Shi Y, Zhong G, et al. Oral mRNA delivery using capsule-mediated gastrointestinal tissue injections. Matter. 2022;5(3):975-987.

17. Altreuter DH, Kirtane AR, Grant T, et al. Changing the pill: developments toward the promise of an ultra-long-acting gastroretentive dosage form. Expert Opin Drug Deliv. 2018;15(12):1189-1198.

18. Byrne J, Huang HW, McRae JC, et al. Devices for drug delivery in the gastrointestinal tract: A review of systems physically interacting with the mucosa for enhanced delivery. Adv Drug Deliv Rev. 2021;177:113926.

19. Caffarel-Salvador E, Abramson A, Langer R, et al. Oral delivery of biologics using drug-device combinations. Curr Opin Pharmacol. 2017;36:8-13.

20. Chu JN, Traverso G. Foundations of gastrointestinal-based drug delivery and future developments. Nat Rev Gastroenterol Hepatol. 2022;19(4):219-238.

21. Kirtane AR, Tang C, Freitas D, Bernstock JD, Traverso G. Challenges and opportunities in the development of mucosal mRNA vaccines. Curr. Opin. Immunol. 2023;85:102388

22. Subramanian DA, Langer R, Traverso G. Mucus interaction to improve gastrointestinal retention and pharmacokinetics of orally administered nano-drug delivery systems. J. Nanobiotechnology. 2022;20(1):362

23. Lyndra therapeutics [accessed 2023 November 30] https://lyndra.com/

24. Bellinger AM, Jafari M, Grant TM, et al. Oral, ultra-long-lasting drug delivery: Application toward malaria elimination goals. Sci Transl Med. 2016;8(865):365ra157.

25. Hayward A, Bensel T, Mazdiyasni H, et al. Scalable gastric resident systems for veterinary application. Sci Rep. 2018,8:11816.

26. Kanasty R, Low S, Bhise N, et al. A pharmaceutical answer to nonadherence: once weekly oral memantine for Alzheimer's disease. J Control Rel. 2019;303:34-41.

27. Kirtane AR, Abouzid O, Minahan D, et al. Development of an oral once-weekly drug delivery system for HIV antiretroviral therapy. Nat Commun. 2018;9:2.

28. Kirtane AR, Hua T, Hayward A, et al. A once-a-month oral contraceptive. Sci Transl Med. 2019;11(521): eaay2602.

29. Klausner EA, Lavy E, Friedman M, et al. Expandable gastroretentive dosage forms. J Control Release. 2003;90(2):143-162.

30. Pawar VK, Kansal S, Garg G, et al. Gastroretentive dosage forms: a review with special emphasis on floating drug delivery systems. Drug Deliv. 2011;18(2):97-110.

31. Pawar VK, Kansal S, Asthana S, et al. Industrial perspective of gastroretentive drug delivery systems: Physicochemical, biopharmaceutical, technological and regulatory consideration. Expert Opin Drug Deliv. 2012;9(5):551-565.

32. Prinderre P, Sauzet C, Fuxen C. Advances in gastro retentive drug-delivery systems. Expert Opin Drug Deliv. 2011;8(9):1189-1203.

33. Chaudhari S, Walde S, Purohit A. A review on floating drug delivery systems. Int. J. Pharm. Sci. Res. 2023;81(1):37-41

34. Mahmoud DB, Schulz-Siegmund M. Utilizing 4D printing to design smart gastroretentive, esophageal, and intravesical drug delivery systems. Adv Health Mat. 2022;12(19):2202631.

35. Melocchi A, Uboldi M, Cerea M, et al. Shape memory materials and 4D printing in pharmaceutics. Adv Drug Deliv Rev. 2021a;173:216-237.

36. Verma M, Vishwanath K, Eweje F, et al. A gastric resident drug delivery system for prolonged gram-level dosing of tuberculosis treatment. Sci Transl Med. 2019;11(483):eaau6267.

37. Verma M, Chu JN, Salama JA, et al. Development of a long-acting direct-acting antiviral system for hepatitis c virus treatment in a swine model. Gastroenterol. 2020;158:S-1321.

38. Inverardi N, Scalet G, Melocchi A,et al. Experimental and computational analysis of a pharmaceutical-grade shape memory polymer applied to the development of gastroretentive drug delivery systems. J Mech Behav Biomed Mater. 2021;124:104814.

39. Melocchi A, Inverardi N, Uboldi M, et al. Retentive device for intravesical drug delivery based on water-induced shape memory response of poly(vinil alcohol): design concept and 4D printing feasibility. Int J Pharm. 2019a;559: 299-311.

40. Melocchi A, Uboldi M, Inverardi N, et al. Expandable drug delivery system for gastric retention based on shape memory polymers: development via 4D printing and extrusion. Int J Pharm. 2019b;571:118700.

41. Uboldi M, Melocchi A, Moutaharrik S, et al. Dataset on a small-scale film-coating process developed for self-expanding 4D printed drug delivery devices. Coatings. 2021;11(10):1252.

42. Uboldi M, Pasini C, Pandini S, et al. Expandable drug delivery systems based on shape memory polymers: impact of film coating on mechanical properties and release and recovery performance. Pharmaceutics. 2022;14(12):2814.

43. Uboldi M, Perrotta C, Moscheni C, et al. Insights into the safety and versatility of 4D printed intravesical drug delivery systems. Pharmaceutics. 2023;15(3):757.

44. Uboldi M, Gelain A, Buratti G, et al. Development of 4D printed intravesical drug delivery systems: scale-up of film-coating. J D Deliv Sci Technol. 2023;87:104875.

45. Hatipoglu BA, Rekindling hope for remission: current impact of diabetes for our world's future health and economy. Endocrinol. Metab. Clin. N. Am. 2023;52(1):1-12

46. Baker C, Retzik-Stahr C, Singh V, et al. Should metformin remain the first-line therapy for treatment of type 2 diabetes?. Ther Adv Endocrinol Metab. 2021;12:2042018820980225.

47. Buse JB, DeFronzo RA, Rosenstock J, et al. The primary glucose-lowering effect of metformin resides in the gut, not the circulation: results from short-term pharmacokinetic and 12-week dose-ranging studies. Diabetes Care. 2016;39(2):198-205.

48. Garber AJ, Duncan TG, Goodman AM, et al. Efficacy of metformin in type II diabetes: results of a double-blind, placebo-controlled, dose-response trial fn1. Am J Med. 1997;103(6):491-497.

49. Corcoran C, Jacobs TF. Metformin. Treasure Island (FL): StatPearls Publishing; 2023.

50. Sanchez-Rangel E, Inzucchi SE. Metformin: clinical use in type 2 diabetes. Diabetologia. 2017;60(9):1586-1593.

51. Sheehan MT. Current therapeutic options in type 2 diabetes mellitus: a practical approach. Clin Med Res. 2003;1(3):189-200.

52. Boldhane SP, Kuchekar BS. Gastroretentive drug delivery of metformin hydrochloride: Formulation and in vitro evaluation using 3^2 full factorial design. Current Drug Deliv. 2009;6(5):477-485.

53. Hoffman A, Stepensky D, Lavy E, et al. Pharmacokinetic and pharmacodynamic aspects of gastroretentive dosage forms. Int J Pharm. 2004;277(1-2):141-153.

54. Kim JH, Song SH, Joo SH, et al. Formulation of a gastroretentive in situ oral gel containing metformin HCl based on DoE. Pharmaceutics. 2022;14(9):1777.

55. Pawar R, Jagdale S, Randive D. Development of floating gastroretentive drug delivery system based on a novel excipient for metformin hydrochloride using mixture design. Int J Pharm Pharm Sci. 2020;12(10):62-71.

56. Kumar A, Sharma AK, Dutt R. A Review of gastro-retentive drug delivery systems for

antidiabetics and its present status. Res J Pharm Technol. 2021;14(1):538-546.

57. Upadhyay P, Pandit JK, Upadhyay S, et al. Studies on formulation and optimization of Gastro Retentive multi-Particulates of Glibenclamide and Metformin hydrochloride for the treatment of Type II Diabetes mellitus using Gelucire: A Review. J Pharm Sci Res. 2010;2(6):351-354.
58. Jeong YS, Jusko WJ. Meta-Assessment of metformin absorption and disposition pharmacokinetics in nine species. Pharmaceuticals. 2021;14(6):545.
59. Scheen AJ. Clinical pharmacokinetics of metformin. Clin Pharmacokinet. 1996;30(5):359-371.
60. Stepensky D, Friedman M, Srour W, et al. Preclinical evaluation of pharmacokinetic-pharmacodynamic rationale for oral CR metformin formulation. J Control Release. 2001;71(1):107-115.
61. Aroda VR, Ratner RE. Metformin and type 2 diabetes prevention. Diabetes Spectr. 2018;31(4):336-342.
62. Blough B, Moreland A, Mora A Jr. Metformin-induced lactic acidosis with emphasis on the anion gap. Proc (Bayl Univ Med Cent). 2015;28(1):31-33.
63. Nasri H, Rafieian-Kopaei M. Metformin: current knowledge. J Res Med Sci. 2014;19(7):658-664.
64. Rojas LBA, Gomes MB. Metformin: an old but still the best treatment for type 2 diabetes. Diabetol Metab Syndr. 2013;5(1):6.
65. Hemels M, Jensen RCØ, Toumi M, et al. Relative effectiveness management of type II diabetes in europe: Can the agencies' demands be met? Value Health. 2010;13:A55.
66. Diabetes in Europe [accessed 2023 November 30] https://www.mepinterestgroupdiabetes.eu/wp-content/uploads/2021/11/IDF-Atlas-Factsheet-2021_EUR.pdf
67. IDF Diabetes Atlas [accessed 2023 November 30] https://diabetesatlas.org/data/en/indicators/17/
68. Jönsson B. Revealing the cost of Type II diabetes in Europe. Diabetologia. 2002;45(7):S5–S12.

69. Völzke H, Ittermann T, Schmidt CO, et al. Prevalence trends in lifestyle-related risk factors. Dtsch Arztebl Int. 2015;112(11):185-192.

70. Zhuo X, Zhang P, Hoerger TJ. Lifetime direct medical costs of treating type 2 diabetes and diabetic complications. Am J Prev Med. 2013;45(3):253-261.

71. Ferry JD. Viscoelastic Properties of Polymers. New York (NY): John Wiley & Sons; 1980.

72. Daskalakis E, Hassan MH, Omar AM, et al. Accelerated degradation of poly-ε-caprolactone composite scaffolds for large bone defects. Polymers. 2023;15(3):670.

73. Lee SH, Lee JH, Cho, YS. Analysis of degradation rate for dimensionless surface area of well-interconnected PCL scaffold via in-vitro accelerated degradation experiment. Tissue Eng Regen Med. 2014;11:446-452.

74. Zhou ZX, Chen YR, Zhang JY, et al. Facile strategy on hydrophilic modification of poly(ε-caprolactone) scaffolds for assisting tissue-engineered meniscus constructs in vitro. Front Pharmacol. 2020;11:471.

75. Dumpa N, Butreddy A, Wang H, et al. 3D printing in personalized drug delivery: An overview of hot-melt extrusion-based fused deposition modeling. Int J Pharm. 2021;600:120501.

76. Kallakunta VR, Sarabu S, Bandari S, et al. An update on the contribution of hot-melt extrusion technology to novel drug delivery in the twenty-first century: part I. Expert Opin Drug Deliv. 2019;16(5):539-550.

77. Sarabu S, Bandari S, Kallakunta VR, et al. An update on the contribution of hot-melt extrusion technology to novel drug delivery in the twenty-first century: part II. Expert Opin Drug Deliv. 2019;16(6):567-582.

78. Simões MF, Pinto RMA, Simões S. Hot-melt extrusion in the pharmaceutical industry: toward filing a new drug application. Drug Discov Today. 2019;24(9):1749-1768.

79. Zema L, Loreti G, Melocchi A, et al. Injection molding and its application to drug delivery. J Control Release. 2012;159(3):324-331.

80. Dash TK, Konkimalla VB, Poly-ϵ-caprolactone based formulations for drug delivery and tissue engineering: A review, J. Control release 2012; 158(1) 15-33

81. Elbjorn M, Provencio J, Phillips P, et al. An Innovative polymeric platform for controlled and localized drug delivery. Pharmaceutics. 2023;15(7):1795.

82. Henderson B. Polycaprolactones: properties, applications, and selected research. London (UK): Nova Science Publishers; 2017.

83. Malikmammadov E, Tanir TE, Kiziltay A, et al. PCL and PCL-based materials in biomedical applications. J Biomater Sci Polym Ed. 2018;29(7-9):863-893.

84. Mohamed R, Yusoh K. A Review on the recent research of polycaprolactone (PCL). Adv Mat Res. 2015;1134:249-255.

85. Mondal D, Griffith M. Venkatraman S.S.) Polycaprolactone-based biomaterials for tissue engineering and drug delivery: Current scenario and challenges, Int. J. Polym. Mater., 2016;65(5): 255-265

86. Faglie A, Emerine R, Chou S-F. Effects of poloxamers as excipients on the physicomechanical properties, cellular biocompatibility, and in vitro drug release of electrospun polycaprolactone (PCL), Fibers Polyms. 2023;15(14):2997.

87. Douglas P, Andrews G,. Jones D, Walker G, Analysis of in vitro drug dissolution from PCL melt extrusion, Chem. Eng. J.2010; 164(2–3): 359-370

88. Guastaferro M, Baldino M, Cardea S, Reverchon E. Supercritical processing of PCL and PCL-PEG blends to produce improved PCL-based porous scaffolds, J. Supercrit. Fluids, 2022; 186:105611

89. Dalton M, Ebrahimi F, Xu H, et al. The influence of the molecular weight of poly(ethylene oxide) on the hydrolytic degradation and physical properties of polycaprolactone binary blends. Macromol. 2023;3(3):431-450.

90. Douglas P, Albadarin AB, Sajjia M, et al. Effect of poly ethylene glycol on the mechanical and thermal properties of bioactive poly(ε-caprolactone) melt extrudates for pharmaceutical applications. Int J Pharm. 2016;500(1-2):179–186.

91. Homaeigohar S, Boccaccini AR. Nature-derived and synthetic additives to poly(ε-caprolactone) nanofibrous systems for biomedicine; an updated overview. Front Chem. 2022;19:809676.

92. Bezerra GSN, De Lima GG, Colbert DM et al. Micro-injection moulding of PEO/PCL blend–based matrices for extended oral delivery of fenbendazole. Pharmaceutics. 2023; 15(3):900.

93. Bezerra GSN, de Lima TADM, Colbert DM et al. Formulation and evaluation of fenbendazole extended-release extrudes processed by hot-melt extrusion. Polymers. 2022;14:4188

94. Berger V, Green Buzhor M, Evstafeva D et al. 3D printing of a controlled urea delivery device for the prevention of tooth decay, Int. J. Pharm. 2023; 631:122528,

95. Vlachou M, Siamidi A, Anagnostopoulou D, et al. Tuning the release of the pineal hormone melatonin via poly(ε-caprolactone)-based copolymers matrix tablets.J. Drug Deliv. Sci.Technol. 2023;79:04051

96. Bartnikowski M, Dargaville TR, Ivanovski S, et al. Degradation mechanisms of polycaprolactone in the context of chemistry, geometry and environment. Prog Polym Sci. 2019;96:1-20.

97. Evonik Leading Beyond Chemistry [accessed 2023 November 30]. https://healthcare.evonik.com/en/medical-devices/bioresorbable-polymers/standard-polymers

98. Sun H, Mei L, Song C, et al. The in vivo degradation, absorption and excretion of PCL-based implant. Biomaterials. 2006;27(9):1735-1740.

99. Balguri SP, Adelli GR, Tatke A, et al. Melt-cast noninvasive ocular inserts for posterior segment drug delivery. J Pharm Sci. 2017;106(12):3515-3523.

100. Blackwell CJ, Haernvall K, Guebitz GM et al. Enzymatic Degradation of star poly(ε-caprolactone) with different central units. Polymers. 2018; 10(11):1266.

101. Castilla-Cortázar I, Más-Estellés J, Meseguer-Dueñas JM et al. Hydrolytic and enzymatic degradation of a poly(ε-caprolactone) network. Polym. Degrad. Stab. 2012; 97(8):1241-1248,

102. Gan Z, Liang Q, Zhang J et al. Enzymatic degradation of poly(ε-caprolactone) film in phosphate buffer solution containing lipases, Polym. Degrad. Stab. 1997; 56(2):209-213

103. Pastorino L, Pioli F, Mario Zilli et al. Lipase-catalyzed degradation of poly(ε-caprolactone). Enzyme Microb. Technol. 2004;35(4): 321-326

104. Liu M, Zhang T, Long L et al. Efficient enzymatic degradation of poly (3-caprolactone) by an engineered bifunctional lipase-cutinase. Polym. Degrad. Stabil., 2019; 160:120-125

105. Woodruff MA, Hutmacher DW. The return of a forgotten polymer–polycaprolactone in the 21st century. Prog. Polym. Sci. 2010; 35(10):1217-1256

106. Chen DR, Bei JZ, Wang SG. Polycaprolactone microparticles and their biodegradation. Polym. Degrad. Stab. 2000; 67(3):455-459.

107. Bartnikowski M, Dargaville TR, Ivanovski S et al. Degradation mechanisms of polycaprolactone in the context of chemistry, geometry and environment. Prog. Polym. Sci., 2019; 96:1-20

108. Hoshino A, Isono Y. Degradation of aliphatic polyester films by commercially available lipases with special reference to rapid and complete degradation of poly(L-lactide) film by lipase PL derived from Alcaligenes sp. Biodegradation. 2002; 13:141-147

109. Cheng L, Lei L, Guo S. In vitro and in vivo evaluation of praziquantel loaded implants based on PEG/PCL blends, Int. J. Pharm. 2010; 387(1-2): 129-138

110. Dalton M, Ebrahimi F, Xu H, Gong K et al., The Influence of the molecular weight of poly(ethylene oxide) on the hydrolytic degradation and physical properties of polycaprolactone binary blends. *Macromol*. 2023; 3(3):431-450.

111. Jiang Y, Mao K, Cai X, Lai S, Chen S. Poly(ethyl glycol) assisting water sorption enhancement of poly(ε-caprolactone) blend for drug delivery, J. Appl. Polym. Sci. 2011;122(4):2309-2316

112. Sun H, Mei L, Song C, Cui X, Wang P. The in vivo degradation, absorption and excretion of PCL-based implant, Biomaterials, 2006;27(9): 1735-1740

113. Chang HI, Williamson MR, Perrie Y et al. Precipitation casting of drug-loaded microporous PCL matrices: Incorporation of progesterone by co-dissolution. J. Control. Release. 2005; 106(3)263-272.

114. Asvadi NH., Dang NTT., Davis-Poynter N. et al., Evaluation of microporous polycaprolactone matrices for controlled delivery of antiviral microbicides to the female genital tract, J. Mater. Sci. Mater. Med. 2013; 24(12): 2719-2727

115. Dang NTT., Turner MS., Coombes AGA. Development of intra-vaginal matrices from polycaprolactone for sustained release of antimicrobial agents, J. Biomater. Appl. 2013;28(1):74-83

116. Wong BS, Teoh SH, Kang L. Polycaprolactone scaffold as targeted drug delivery system and cell attachment scaffold for postsurgical care of limb salvage. Drug Deliv Transl Res. 2012; 2(4):272-283

117. Chattopadhyay DK, Webster DC. Thermal stability and flame retardancy of polyurethanes. Prog Polym Sci. 2009;34(10):1068-1133.

118. Das A, Mahanwar P. A brief discussion on advances in polyurethane applications. Adv Ind Eng Polym Res. 2020;3(3):93-101.

119. Petrović ZS, Ferguson J. Polyurethane elastomers. Prog Polym Sci. 1991;16(5): 695-836.

120. Xie F, Zhang T, Bryant P, et al. Degradation and stabilization of polyurethane elastomers. Progress Poly Sci. 2019;90:211-268.

121. Cherng JY, Hou TY, Shih MF, et al. Polyurethane-based drug delivery systems. Int J Pharm. 2013;450(1-2):145-162.

122. Claeys B, Vervaeck A, Hillewaere XKD, et al. Thermoplastic polyurethanes for the manufacturing of highly dosed oral sustained release matrices via hot melt extrusion and injection molding. Eur J Pharm Biopharm. 2015;90:44-52.

123. St John KR. The use of polyurethane materials in the surgery of the spine: a review. Spine J. 2014; 14(12):3038-3047.

124. Joseph J, Patel RM, Wenham A, et al. Biomedical applications of polyurethane materials and coatings. Trans Inst Met. 2018;96(3):121-129.

125. Koutsamanis I, Roblegg E, Spoerk M. Controlled delivery via hot-melt extrusion: a focus on non-biodegradable carriers for non-oral applications. J Drug Deliv Sci Technol. 2023;81:104289.

126. M'Bengue MS, Mesnard T, Chai F, et al. Evaluation of a medical grade thermoplastic polyurethane for the manufacture of an implantable medical device: the impact of FDM 3D-printing and gamma sterilization. Pharmaceutics. 2023;15(2):456.

127. Verstraete G, Van Renterghem J, Van Bockstal PJ, et al. Hydrophilic thermoplastic polyurethanes for the manufacturing of highly dosed oral sustained release matrices via hot melt extrusion and injection molding. Int J Pharm. 2016;506(1-2):214-221.

128. Verstraete G, Samaro A, Grymonpré W, et al. 3D printing of high drug loaded dosage forms using thermoplastic polyurethanes. Int J Pharm. 2018;536(1):318-325.

129. Wendels S, Avérous L. Biobased polyurethanes for biomedical applications. Bioact Mater. 2021;6(4):1083-1106.

130. Cailleaux S, Sanchez-Ballester NM, Gueche YA, et al. Fused Deposition Modeling (FDM), the new asset for the production of tailored medicines. J Control Release. 2021;330:821-841.

131. Melocchi A, Uboldi M, Briatico-Vangosa F, et al. The chronotopic™ system for pulsatile and colonic delivery of active molecules in the era of precision medicine: Feasibility by 3D printing via fused deposition modeling (FDM). Pharmaceutics. 2021;13(5):759.

132. Parulski C, Jennotte O, Lechanteur A, et al. Challenges of fused deposition modeling 3D printing in pharmaceutical applications: Where are we now?. Adv Drug Deliv Rev. 2021;175:13810.

133. Kong F, Singh RP. A human gastric simulator (HGS) to study food digestion in human stomach. J Food Sci. 2010;75(9):E627-35.

Table 1: Printing parameters set for the different filaments in use.

	TPU 7	TPU 8	TPU 9	PLA
Nozzle temperature (°C)	215	220	220	220
Build plate temperature (°C)	40			
Fan speed (%)	0	0	50	100
Printing speed (mm/s)	15	30	30	70
Retraction (mm)	0	0	4.2	2.2
Number of perimeters	1			2
Layer height (mm)	0.2			0.15
Infill (%)	100			100
Infill type	Rectilinear			

Table 2: Composition (% by weight) of the GREDDS cores.

Metformin	PCL	PEG 4000	PEG 8000	PEO
50	50			
25	75			
50	40	10		
50	40		10	
50	40			10
50	25	25		
50	25		25	

Table 3: Fitting parameters relevant to the Korsmeyer-Peppas model.

	n	n LoConf*	n UpConf**	R^{2***}
25% metformin + 75% PCL	0.514	0.487	0.541	0.939
50% metformin + 50% PCL	0.500	0.494	0.506	0.997
50% meformin + 40% PCL + 10% PEG8000	0.802	0.720	0.883	0.992
50% meformin + 25% PCL + 25% PEG8000	0.562	0.198	0.926	0.997
50% meformin + 40% PCL + 10% PEG4000	0.684	0.632	0.736	0.996
50% meformin + 25% PCL + 25% PEG4000	0.510	0.256	0.763	0.998
50% meformin + 40% PCL + 10% PEO	0.593	0.549	0.637	0.994

* 95% Lower confidence limit of exponent n

** 95% Upper confidence limit of exponent n

*** Regression correlation coefficient

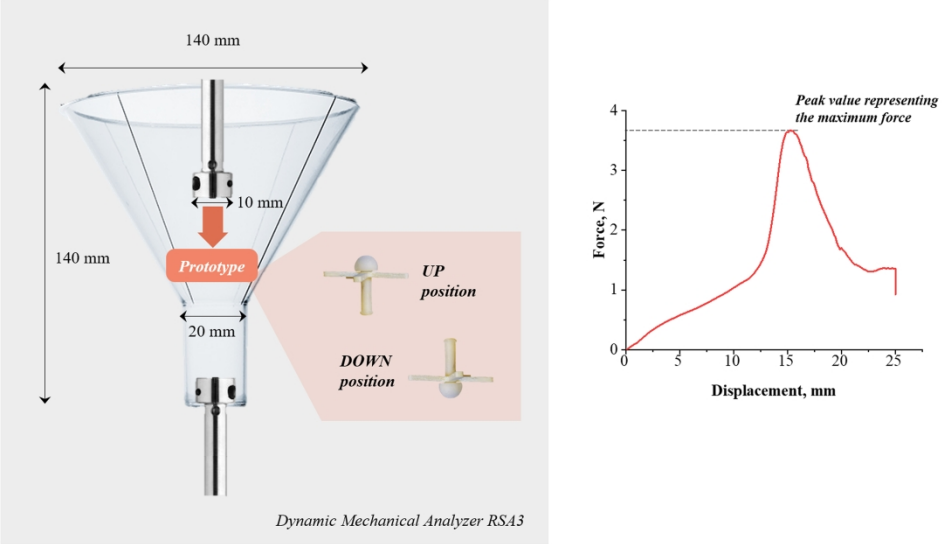

Figure 1: Outline of the funnel experiment set-up together with an example of the resulting curve.

189x111mm (500 x 500 DPI)

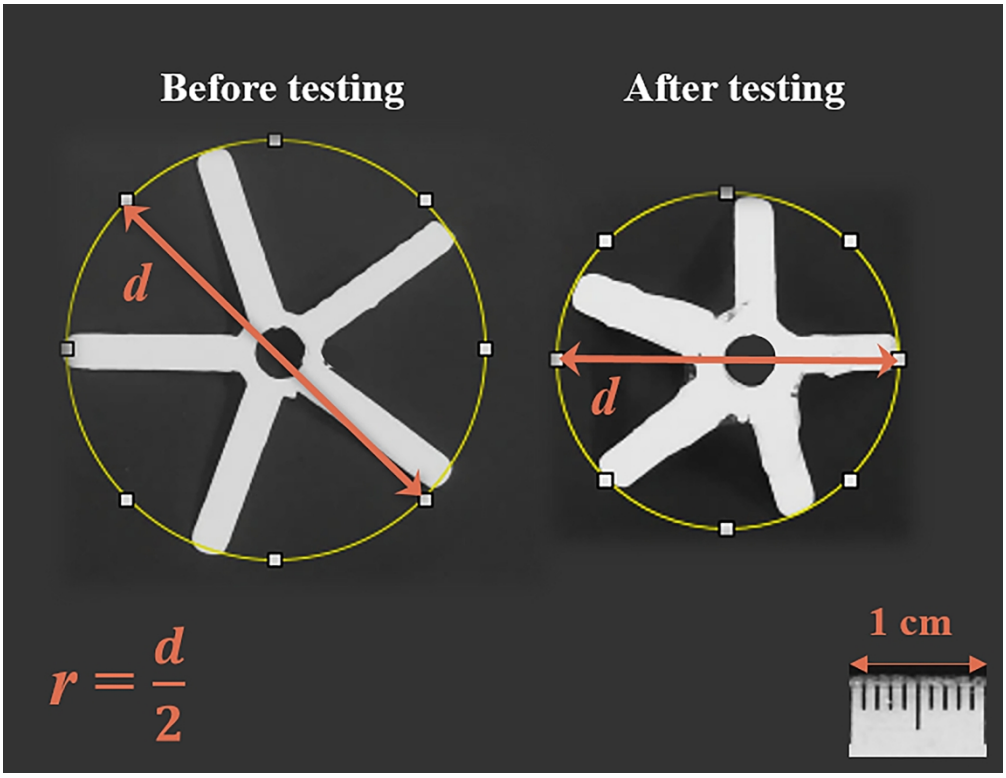

Figure 2: Photographs taken from above on a TPU-based umbrella-like skeleton before the experiment and retrieved at the end of the opening test, even if not fully deployed, highlighting the procedure for determining the radius.

90x69mm (500 x 500 DPI)

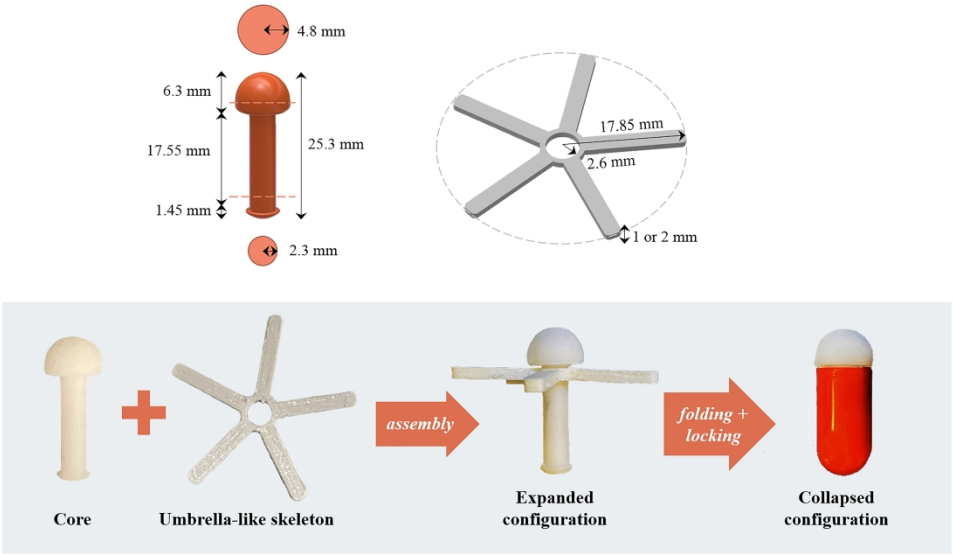

Figure 3: Electronic models and resulting photographs of the main components of the GREDDS, upon assembly and after insertion into a commercially available capsule body.

189x113mm (500 x 500 DPI)

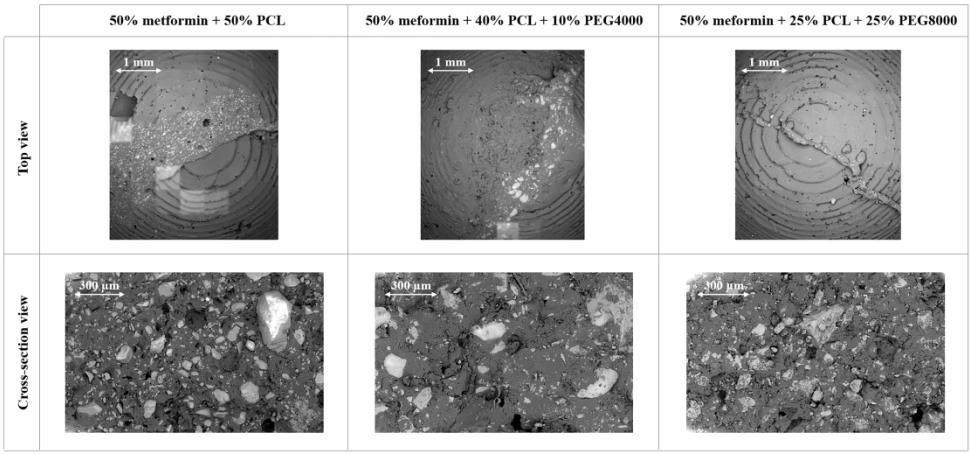

Figure 4: SEM photomicrographs (top and cross-section view) of different PCL-based cores.

189x91mm (600 x 600 DPI)

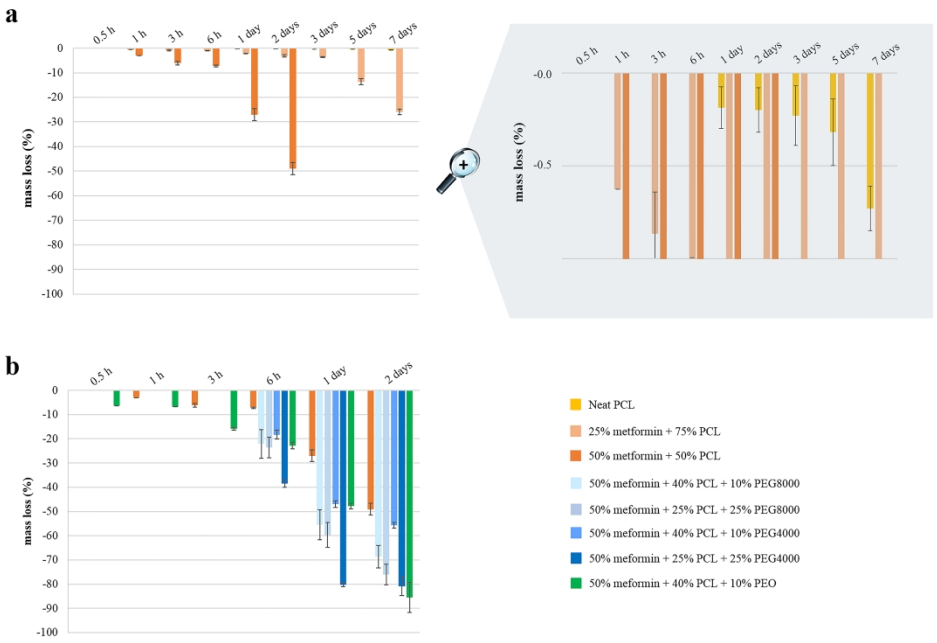

Figure 5: Mass loss data relevant to specimens a) based on neat PCL and loaded with either 25 and 50% of metformin or b) containing 50% of the drug and different amounts of soluble adjuvants.

189x132mm (500 x 500 DPI)

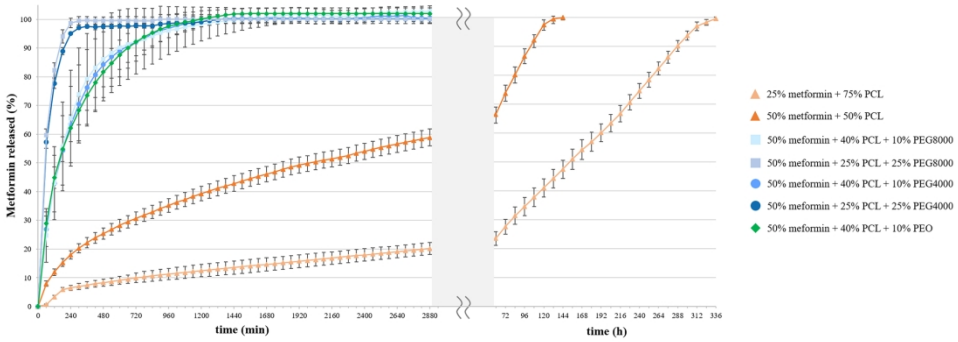

Figure 6: Release profiles relevant to different PCL-based cores.

189x73mm (300 x 300 DPI)

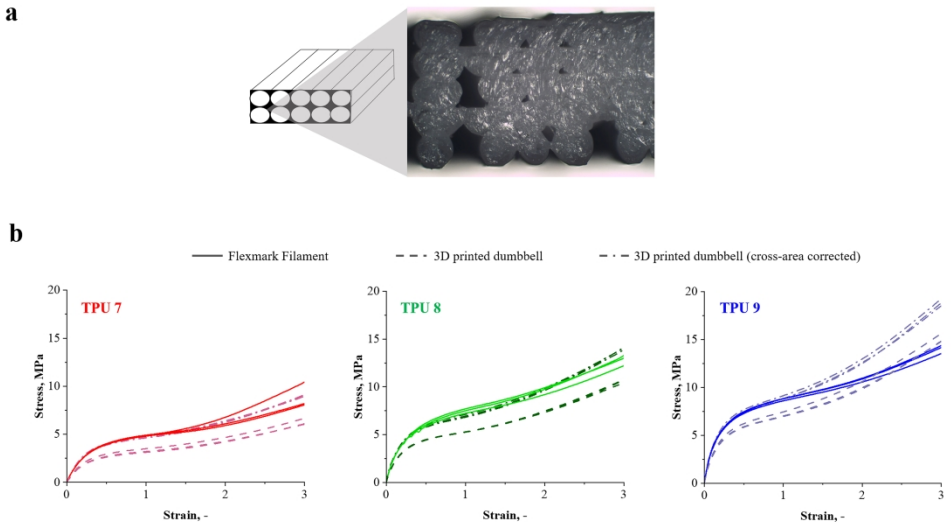

Figure 7: a) Outline and photomicrograph of the cross-section of a printed TPU 7-based dumbbell and b) stress-strain curves relevant to various TPU filaments, compared to the resulting printed specimens. In the last case the stress values were also corrected for the actual cross-area (i.e. by excluding voids).

189x106mm (500 x 500 DPI)

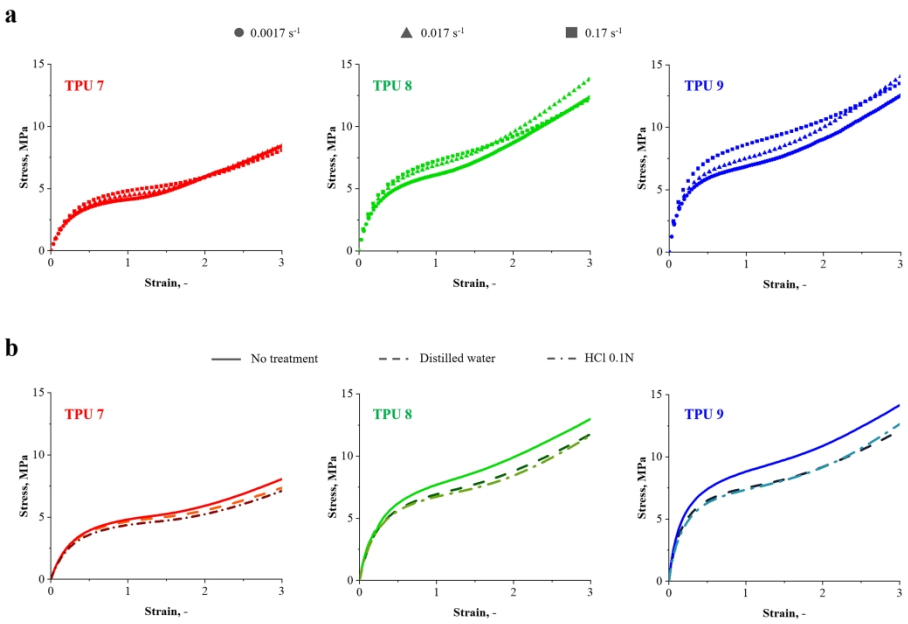

Figure 8: Stress-strain curves relevant to various TPU filaments tested a) at increasing strain rated and b) upon exposure to diverse environmental conditions.

189x124mm (500 x 500 DPI)

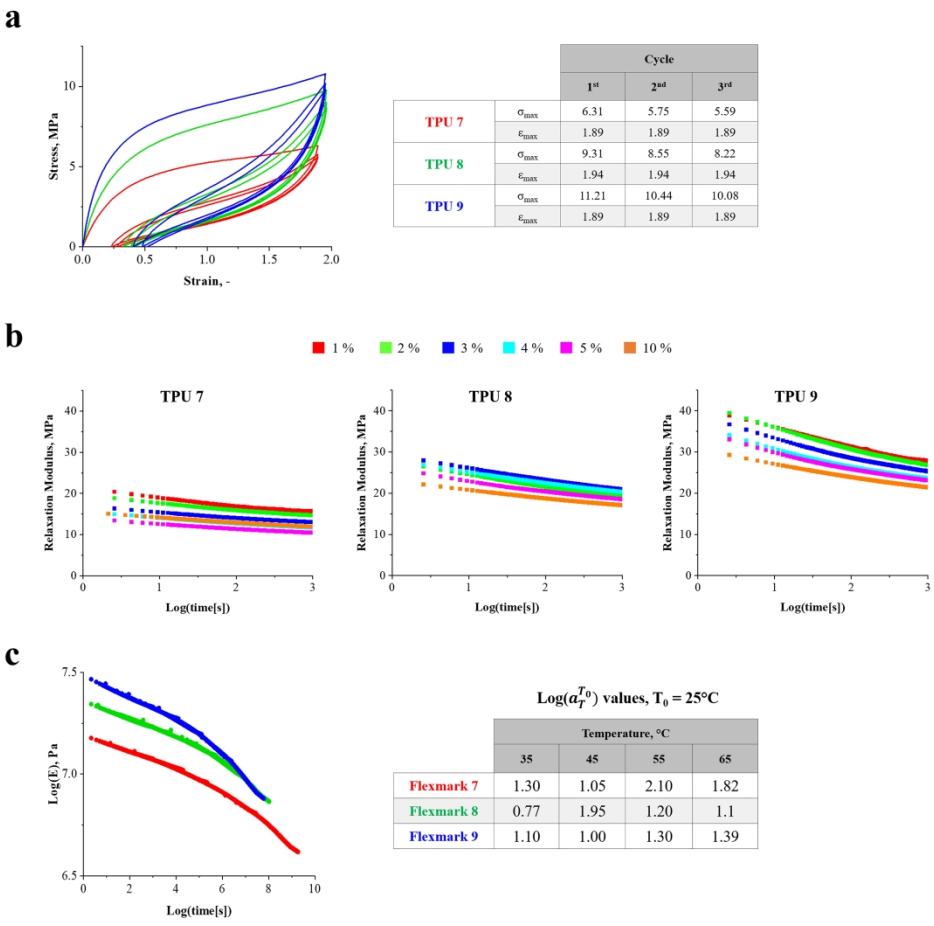

		Cycle		
		1st	2nd	3rd
TPU 7	σ_{max}	6.31	5.75	5.59
	ε_{max}	1.89	1.89	1.89
TPU 8	σ_{max}	9.31	8.55	8.22
	ε_{max}	1.94	1.94	1.94
TPU 9	σ_{max}	11.21	10.44	10.08
	ε_{max}	1.89	1.89	1.89

$\text{Log}(a_T^{T_0})$ values, $T_0 = 25°C$

	Temperature, °C			
	35	45	55	65
Flexmark 7	1.30	1.05	2.10	1.82
Flexmark 8	0.77	1.95	1.20	1.1
Flexmark 9	1.10	1.00	1.30	1.39

Figure 9: a) Loading-unloading stress-strain curves, b) relaxation modulus under different temperature conditions and at increasing strain values versus log-time curves and c) resulting master curves (shift factors details in table) relevant to various TPU filaments.

189x182mm (500 x 500 DPI)

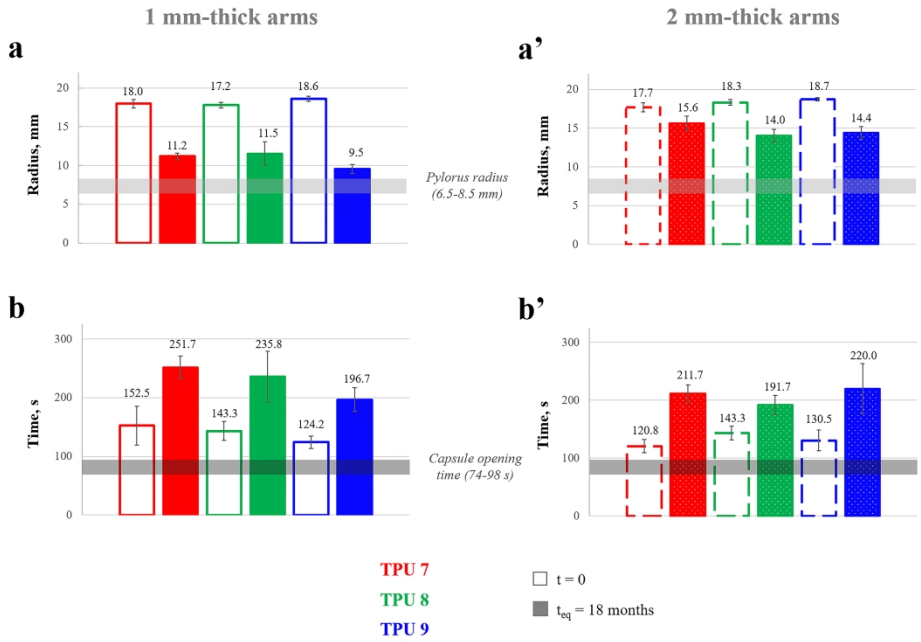

Figure 10: Radius (a, a') and opening time (b, b') data relevant to 1- and 2-mm thick umbrella-like skeletons based on various TPUs, tested upon insertion into commercially-available capsules and at increasing storage times.

189x130mm (500 x 500 DPI)

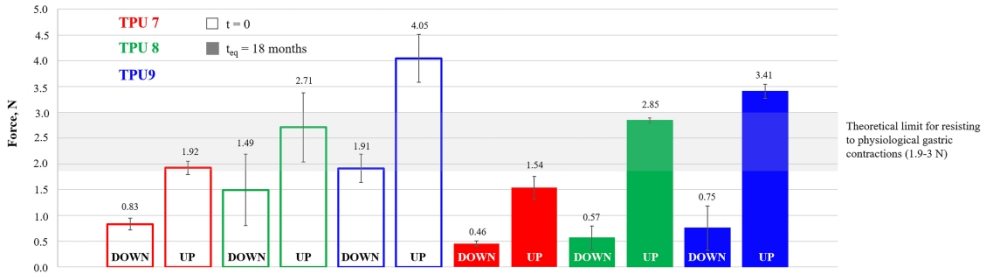

Figure 11: Maximum forces registered during the funnel test relevant to assembled GREDDS entailing 2 mm thick umbrella-like skeletons based on various TPUs and tested at increasing storage times.

189x68mm (500 x 500 DPI)

Figure 1: Outline of the funnel experiment set-up together with an example of the resulting curve.

Figure 2: Photographs taken from above on a TPU-based umbrella-like skeleton before the experiment and retrieved at the end of the opening test, even if not fully deployed, highlighting the procedure for determining the radius.

Figure 3: Electronic models and resulting photographs of the main components of the GREDDS, upon assembly and after insertion into a commercially available capsule body.

Figure 4: SEM photomicrographs (top and cross-section view) of different PCL-based cores.

Figure 5: Mass loss data relevant to specimens a) based on neat PCL and loaded with either 25 and 50% of metformin or b) containing 50% of the drug and different amounts of soluble adjuvants.

Figure 6: Release profiles relevant to different PCL-based cores.

Figure 7: a) Outline and photomicrograph of the cross-section of a printed TPU 7-based dumbbell and b) stress-strain curves relevant to various TPU filaments, compared to the resulting printed specimens. In the last case the stress values were also corrected for the actual cross-area (*i.e.* by excluding voids).

Figure 8: Stress-strain curves relevant to various TPU filaments tested a) at increasing strain rated and b) upon exposure to diverse environmental conditions.

Figure 9: a) Loading-unloading stress-strain curves, b) relaxation modulus under different temperature conditions and at increasing strain values *versus* log-time curves and c) resulting master curves (shift factors details in table) relevant to various TPU filaments.

Figure 10: Radius (a, a') and opening time (b, b') data relevant to 1- and 2-mm thick umbrella-like skeletons based on various TPUs, tested upon insertion into commercially-available capsules and at increasing storage times.

Figure 11: Maximum forces registered during the funnel test relevant to assembled GREDDS entailing 2 mm thick umbrella-like skeletons based on various TPUs and tested at increasing storage times.